Int. J. Fuzzy Syst. (2022) 24(1):57–72
https://doi.org/10.1007/s40815-021-01115-9

Electrically Stimulated Lower Limb using a Takagi-Sugeno Fuzzy Model and Robust Switched Controller Subject to Actuator Saturation and Fault under Nonideal Conditions

Willian Ricardo Bispo Murbak Nunes[1] · Uiliam Nelson Lendzion Tomaz Alves[2] · Marcelo Augusto Assunção Sanches[3] · Marcelo Carvalho Minhoto Teixeira[4] · Aparecido Augusto de Carvalho[3]

Received: 7 November 2020 / Revised: 9 March 2021 / Accepted: 12 May 2021 / Published online: 10 July 2021

Abstract Electrically stimulated lower limb systems contain higher order nonlinearities and uncertainties in their physical parameters. Takagi-Sugeno (TS) fuzzy models are used to model nonlinear systems. Techniques such as parallel distributed compensation (PDC) are dependent on the membership functions that constitute the TS fuzzy model. When the exact representation approach is used to electrical stimulation applications, the system's performance under PDC control can be deteriorated, because the membership functions may be uncertain, besides a high computational cost be required to compute them. In this paper, we propose a robust switched control subject to actuator saturation and fault (RSwASF) that effectively handles system uncertainties and nonidealities, such as fatigue, spasms, tremor, and muscle recruitment. Control techniques based on TS fuzzy modeling (PDC and robust PDC), as well as other approaches, such as sliding-mode control, backstepping, super-twisting, gain-scheduling, and proportional-integral-derivative (PID) control were compared to RSwASF through the root-mean-squared error (RMSE). The results indicate that RSwASF minimizes the influence of the parametric uncertainties and presents the lowest RMSE for healthy and paraplegic individuals.

Keywords Uncertain nonlinear system · Uncertain fuzzy models · Linear matrix inequalities (LMIs) · Robust switched control · Functional electrical stimulation (FES) · Rehabilitation

✉ Willian Ricardo Bispo Murbak Nunes
willianr@utfpr.edu.br

Uiliam Nelson Lendzion Tomaz Alves
uiliam.alves@ifpr.edu.br

Marcelo Augusto Assunção Sanches
marcelo.sanches@unesp.br

Marcelo Carvalho Minhoto Teixeira
marcelo.minhoto@unesp.br

Aparecido Augusto de Carvalho
aa.carvalho@unesp.br

[1] Control and Automation Laboratory, Federal University of Technology - Paraná (UTFPR), Marcilio Dias St., 635., Apucarana, PR, Brazil

[2] Department of Control and Automation Engineering, Federal Institute of Education, Science and Technology of Paraná (IFPR), Dr. Tito Ave., 801, Jacarezinho, PR, Brazil

[3] Instrumentation & Biomedical Engineering Laboratory, São Paulo State University (UNESP), Prof. José Carlos Rossi Ave., Ilha Solteira, SP 1370, Brazil

[4] Control Research Laboratory, São Paulo State University (UNESP), Prof. José Carlos Rossi Ave., Ilha Solteira, SP 1370, Brazil

1 Introduction

Every year, thousands of people around the world suffer from spinal cord injuries resulting from traffic accidents, acts of violence, or falls. A widely used method for motor rehabilitation is neuromuscular electrical stimulation, promoting the health and welfare of these individuals.

Current research efforts in this field are focused on enhancing the stimulation systems by improving the controllers used in the closed-loop system. Electrical stimulation can act under different purposes and application to the body. For example, in the case of lower limbs, functional electrical stimulation (FES) can be used for motor rehabilitation through knee joint control [1–7], standing up [8–11], sitting pivot transfer [12–14], walking [15–22], swimming [23, 24], rowing [25, 26], and cycling [27–30], among others. In the current state-of-the-art, even simple

motor activities still present great challenges and arouse interest due to the therapeutic benefits derived from electrical stimulation [31].

In this sense, several studies have been recently proposed to regulate knee joint using techniques such as proportional-integral-derivative (PID) control [1, 32], neural networks [33, 34], fuzzy [3, 4, 35], predictive [5, 36], adaptive [7, 37], sliding-mode control [1, 38, 39], robust control [6, 7], switched control [6], among others. About the recent papers, a robust parallel distributed compensation (RPDC) was proposed by Covacic et al. [35] considering norm-bounded uncertainties. However, it does not deal with uncertain nonlinear functions. Gaino et al. [3] presented a PDC discretized by emulation around a single operating point. However, it has limitations for practical applications, and its design does not consider plant uncertainties. Teodoro et al. [6] evaluated the performance of switched and robust controllers, for an uncertain linear model of electrical stimuli applied to the angular position control of a knee, which presents an uncertain term added to the control signal. Although these authors obtained interesting results, the technique is linear and does not consider the saturation and fault of the actuator. Kirsch et al. [5] presented a predictive control model for knee extension aiming to minimize muscular fatigue. However, the performance of the predictive controller for steady-state regulation was not been satisfactory for a longer time. Finally, Gaino et al. [4] proposed a PDC based on the TS fuzzy model that is capable of regulation at different operating points. However, it assumes ideal conditions in its simulations and does not consider the uncertainties of the plant and other practical aspects.

The major challenge addressed by this paper is the achievement of regulation in the presence of nonlinear behavior and/or uncertainties in the musculoskeletal complex. Another significant issue is the nonlinear effect of actuator saturation in the control design. Most authors do not consider the saturation effects. The absence of saturation effects in the control design impacts the performance results. The current trend in medical devices is miniaturization, wearability, and low energy consumption. Therefore, it is important to consider the system behavior when the actuator fails or experiences a decrease in power due to limitations in the power source.

This study contributes to the state-of-the-art by improving the steady-state regulation results by switched control, considering fatigue, spasms, tremor, muscular recruitment, and actuator fault as plant uncertainties in an operating region. Although the system has several nonlinearities and uncertainties, the proposed technique uses an exact TS fuzzy model, but does not depend on the membership functions, which are uncertain in this case.

To the best of our knowledge, this is the first study in which a switched controller subject to saturation using TS fuzzy models was used in electrical stimulation of lower limbs under nonideal conditions. The control design is based on linear matrix inequalities (LMIs) for a nonideal uncertain plant described by TS fuzzy model with inaccurate membership functions. In relation to the literature, the nondependence of uncertain membership functions is a differential of this study for electrical stimulation applications. For the first time, the robust switched control technique is proposed for electrical stimulation applications considering saturation and fault in the actuator. Moreover, severe intensity levels of fatigue, spasms, and tremor are presented. In addition, the results of other TS fuzzy control techniques are reproduced and evaluated. Finally, we compare our results with those obtained with other important techniques. The results indicate that the proposed switched control presents the lowest RMS error.

The rest of this paper is organized as follows. Sect. 2 presents the derivation of the torque-based nonlinear dynamic model for leg extension, using electrical stimulation, and the TS fuzzy modeling technique. Sect. 3 describes the switched control design subject to actuator saturation using LMIs conditions. Sect. 4 presents the simulation results that demonstrate the controller performance improvement when compared with PDC in dealing with actuator fault, muscle activation uncertainty, and nonidealities like fatigue, spasms, and tremor. Sect. 5 concludes this study.

1.1 Notations

For a matrix $\mathbf{X}$, $\mathbf{X}^{-1}$ and $\mathbf{X}^{T}$ denote the inverse and the transpose of $\mathbf{X}$, respectively. The symbol $\otimes$ denotes the Kronecker product. The symbol $\mathbf{sl}_{p,j} \in \mathbb{R}^{1\times p}$ denotes a row vector whose j-th element is 1 and the others are equal to zero, and $\overrightarrow{\overrightarrow{p}} = p2^{p-1}$, $p \geqslant 1$. For a symmetric matrix, the symbol $*$ denotes the symmetric blocks in relation to the main diagonal. The set $\mathbb{I}_k = \{1,\ 2,\ \cdots,\ k\}$, $k \in \mathbb{N}$. $\|\breve{\boldsymbol{\nu}}\|_{\infty} = \max_{i\in\mathbb{I}_k}|\breve{\boldsymbol{\nu}}_i|$ is the infinity norm of the vector $\breve{\boldsymbol{\nu}}$. Let $\mathrm{co}\{\mathbf{v}_1,\ \mathbf{v}_2,\ \cdots,\mathbf{v}_p\}$ denote the convex hull of the vectors $\mathbf{v}_i$, that is, $\mathbf{v} \in \mathrm{co}\{\mathbf{v}_1, \mathbf{v}_2, \cdots, \mathbf{v}_p\}$ if and only if $\mathbf{v} = \sum_{i=1}^{p} \lambda_i \mathbf{v}_i$, $\lambda_i \geqslant 0$ and $\sum_{i=1}^{p} \lambda_i = 1$, $i \in \mathbb{I}_p = \{1,\ 2,\ \cdots, p\}$. Besides that, $\varsigma = \arg^{*} \min_{i\in\mathbb{I}_{n_r}}\{\mathbf{x_i}\}$ denotes the smallest index $\varsigma \in \mathbb{I}_{n_r}$, such that, for the set $\{\mathbf{x}_1,\ \mathbf{x}_2,\ \cdots, \mathbf{x}_{n_r}\}$, $\mathbf{x}_{\varsigma} = \min_{i\in\mathbb{I}_{n_r}}\{\mathbf{x}_i\}$.

2 Nonlinear Dynamic Model for Leg Extension using Electrical Stimulation

Consider the leg extension system using electrical stimulation with load cell added in the experimental apparatus, whose mathematical model is given by

$$J\ddot{\theta} = H_g(\theta) + \Lambda_p(\theta, \dot{\theta}) + \Gamma_{ke}(M_a); \tag{1}$$

where $\theta, \dot{\theta}, \ddot{\theta}$, and $M_a \in \mathbb{R}$ are angular position, velocity, acceleration, and torque of the lower limb (shank-foot complex), respectively; $J \in \mathbb{R}$ is the moment of inertia, and $H_g(\theta)$ is the gravitational torque, which is given by

$$H_g(\theta) = -mgl\sin(\theta),$$

where m, and $l \in \mathbb{R}$ are the mass and the distance between the knee and the shank-foot complex mass center, respectively, and g is the gravitational acceleration.

The passive musculoskeletal torque of the knee $\Lambda_p(\theta, \dot{\theta})$ is expressed as

$$\Lambda_p(\theta, \dot{\theta}) = -\lambda e^{-E_v\left(\theta+\frac{\pi}{2}\right)}\left(\theta + \frac{\pi}{2} - \omega\right) - B\dot{\theta},$$

where λ and $E_v \in \mathbb{R}$ are the coefficients of the exponential terms related to knee stiffness, $\omega \in \mathbb{R}$ is elastic rest angle of the knee, and $B \in \mathbb{R}$ is the viscous friction coefficient [40].

Concerning the worst scenarios that can occur during electrically stimulated contractions, we incorporate non-idealities indicated in [39, 41]. The FES-induced muscle contraction produces muscular torque $\Gamma_{ke}(M_a)$, which is expressed as

$$\Gamma_{ke}(M_a) = \left(1 + \kappa_{sp} + \kappa_{tr}\right)\kappa_{fat}M_a = \kappa_{stf}M_a,$$

where κ_{sp}, κ_{tr}, and $\kappa_{fat} \in \mathbb{R}$ are related to spasms, tremor, and fatigue, respectively. Three levels of spasms, tremor, and fatigue were taken into account, that is, mild, moderate, and severe. The criterion adopted for the classification of tremor waveforms and muscle spasm was chosen considering its importance in functional movement. For example, the occurrence of spikes in the angular position of the knee referring to spasms is classified as (i) mild, for amplitudes less than 10°; (ii) moderate, for amplitudes between 10° and 20°; and (iii) severe, for amplitudes greater than 20°. Oscillations in the knee position are due to tremors and are classified as: (i) mild, those that modify knee dynamics in amplitude less than 7.5°; (ii) moderate, for amplitude less than 15°; and (iii) severe, for amplitude greater than 15°. The fatigue severity rating was established in such a way that (i) $\kappa_{fat} = 1$ indicates the absence of fatigue; (ii) $0 < \kappa_{fat} < 1$ corresponds to partially fatigued muscle; and (iii) $\kappa_{fat} = 0$ suggests completely fatigued muscle.

Muscle activation M_a can be modeled by a first-order system as follows:

$$\frac{M_a}{\breve{u}_f} = \frac{\hat{G}}{\tau s + 1} \quad \Longleftrightarrow \quad \dot{M}_a = \frac{1}{\tau}\left(-M_a + \hat{G}\breve{u}_f\right),$$

where $\breve{u}_f \in \mathbb{R}$ is the current amplitude of the electrical stimulation, $\tau \in \mathbb{R}$ is time constant of muscle activation, and $\hat{G} \in \mathbb{R}$ is an uncertain parameter [40].

Furthermore, a possible actuator fault is also considered in this paper. The actuator fault is a power loss from the stimulator power supply. In the model, this is represented by $\breve{u}_f(t) = \kappa_{flt}\breve{u}(t)$, which may correspond to the following operating conditions of the actuator: (i) $\kappa_{flt} = 1$ implies that the actuator has no fault; (ii) $0 < \kappa_{flt} < 1$ implies that there is a partial fault in the actuator; and (iii) $\kappa_{flt} = 0$ represents a complete fault in the actuator.

Defining the state variables $\breve{x}_1 = \theta$, $\breve{x}_2 = \dot{\theta}$, and $\breve{x}_3 = M_a$. Then, (1) can be written as follows:

$$\begin{cases} \dot{\breve{x}}_1 = & \breve{x}_2 \\ \dot{\breve{x}}_2 = & \frac{1}{J}\left[-mgl\sin(\breve{x}_1) - \lambda e^{-E_v\left(\breve{x}_1+\frac{\pi}{2}\right)}\left(\breve{x}_1 + \frac{\pi}{2} - \omega\right)\right. \\ & \left. - B\breve{x}_2 + \kappa_{stf}\breve{x}_3\right] \\ \dot{\breve{x}}_3 = & -\frac{1}{\tau}\breve{x}_3 + \frac{\kappa_{flt}\hat{G}}{\tau}\breve{u}. \end{cases} \tag{2}$$

The goal is to maintain the leg angle in a desired position $\breve{x}_1 = \theta = \theta^d$. Considering that the equilibrium point of the system (2) is $\breve{x}_e = [\breve{x}_1 \quad \breve{x}_2 \quad \breve{x}_3]^T = [\theta^d \quad 0 \quad M_a^d]^T$; therefore $\dot{\breve{x}}_1 = 0, \dot{\breve{x}}_2 = 0, \dot{\breve{x}}_3 = 0$, and $\breve{u} = \breve{u}^d$. From (2) it follows that

$$\begin{aligned} 0 = & \frac{1}{J}\left[-mgl\sin(\theta^d) - \lambda e^{-E_v\left(\theta^d+\frac{\pi}{2}\right)}\left(\theta^d + \frac{\pi}{2} - \omega\right)\right. \\ & \left. + \kappa_{stf}M_a^d\right], \\ M_a^d = & \frac{mgl\sin(\theta^d) + \lambda e^{-E_v\left(\theta^d+\frac{\pi}{2}\right)}\left(\theta^d + \frac{\pi}{2} - \omega\right)}{\kappa_{stf}}. \end{aligned}$$

Moreover, define $\breve{u}_f^d = k_{flt}\breve{u}^d$, from (2) one can also obtain

$$\begin{aligned} 0 = & -\frac{1}{\tau}M_a^d + \frac{\hat{G}}{\tau}\breve{u}_f^d, \\ \breve{u}^d = & \frac{\breve{u}_f^d}{k_{flt}} = \frac{M_a^d}{\kappa_{flt}\hat{G}}, \\ = & \frac{mgl\sin(\theta^d) + \lambda e^{-E_v\left(\theta^d+\frac{\pi}{2}\right)}\left(\theta^d + \frac{\pi}{2} - \omega\right)}{\kappa_{stf}\kappa_{flt}\hat{G}}. \end{aligned} \tag{3}$$

In addition, note that the equilibrium point is not the origin $[\breve{x}_1 \quad \breve{x}_2 \quad \breve{x}_3]^T = [0 \quad 0 \quad 0]^T$. Thus, for stability analysis, it is necessary to modify the coordinates as

$x_1 = \check{x}_1 - \theta^d, x_2 = \check{x}_2, x_3 = \check{x}_3 - M_a^d, u = \check{u} - \check{u}^d$ *i.e.*,
$\check{x}_1 = x_1 + \theta^d, \check{x}_2 = x_2, \check{x}_3 = x_3 + M_a^d, \check{u} = u + \check{u}^d$.

It follows that $\dot{x}_1 = \dot{\check{x}}_1$, $\dot{x}_2 = \dot{\check{x}}_2$, and $\dot{x}_3 = \dot{\check{x}}_3$, so

$$\dot{\mathbf{x}}(t) = \begin{bmatrix} 0 & 1 & 0 \\ f_{21}(\mathbf{z}) & -\frac{B}{J} & f_{23}(\mathbf{z}) \\ 0 & 0 & -\frac{1}{\tau} \end{bmatrix} \mathbf{x}(t) + \begin{bmatrix} 0 \\ 0 \\ g_{31}(\mathbf{z}) \end{bmatrix} u(t),$$

$$f_{21}(\mathbf{z}) = \frac{1}{Jx_1}\Big[-mgl\sin(x_1+\theta^d) - \lambda e^{-E_v\left(x_1+\theta^d+\frac{\pi}{2}\right)}\left(x_1+\theta^d+\frac{\pi}{2}-\omega\right) + mgl\sin(\theta^d) + \lambda e^{-E_v\left(\theta^d+\frac{\pi}{2}\right)}\left(\theta^d+\frac{\pi}{2}-\omega\right)\Big],$$

$$f_{23}(\mathbf{z}) = \frac{\left(1+\kappa_{sp}+\kappa_{tr}\right)\kappa_{fat}}{J} = \frac{\kappa_{stf}}{J},$$

$$g_{31}(\mathbf{z}) = \frac{\kappa_{flt}\hat{G}}{\tau}, \tag{4}$$

where $z = [x_1 \quad x_3 \quad \hat{G} \quad \theta^d \quad \kappa_{stf} \quad \kappa_{flt}]^T \in \mathbb{R}^6$ and $\mathbf{x} = [x_1 \quad x_2 \quad x_3]^T$.

Note that $\dot{x}_3 = -\frac{1}{\tau}x_3 + g_{31}(\mathbf{z})\check{u}$, $u = \check{u} - \check{u}^d$, and $x_3 = \check{x}_3 - M_a^d$, where $\check{u}^d$ and M_a^d are uncertain values for different operating points θ^d. Section 3 presents the analysis of the control system design, considering the uncertainties in the plant (4).

2.1 TS Fuzzy Models for the Exact Representation of Nonlinear Systems

Consider an uncertain nonlinear system described by

$$\dot{\mathbf{x}}(t) = \mathbf{f}(\mathbf{z}(t))\mathbf{x}(t) + \mathbf{g}(\mathbf{z}(t))\, \boldsymbol{sat}(\mathbf{u}(t)), \tag{5}$$

where $\mathbf{x}(t) \in \mathbb{R}^{n_x}$ is the state vector, $\mathbf{u}(t) \in \mathbb{R}^{n_u}$ is the input vector, $\mathbf{f}(\cdot) : \mathbb{R}^{n_z} \to \mathbb{R}^{n_x \times n_x}$, $\mathbf{g}(\cdot) : \mathbb{R}^{n_z} \to \mathbb{R}^{n_x \times n_u}$, $\mathbf{z}(t) \in \mathbb{R}^{n_z}$ is a vector with premise variables that depends on the state vector $\mathbf{x}(t)$ and uncertain parameters or unknown variables, and $\text{sat}(\mathbf{u}(t)) \in \mathbb{R}^{n_u}$ is the saturation function of the control input.

The sector nonlinearity approach usually employed to construct an exact TS model of a nonlinear system is adequate in a bounded validity domain [42]. A low performance or system instability may occur when the state trajectories do not belong to the validity domain of the model. The validity domain can be represented by a polyhedral set

$$\mathcal{O} \triangleq \left\{\mathbf{x}(t) \in \mathbb{R}^{n_x} : \left|\mathbf{N}_{(h)}\mathbf{x}(t)\right| \leqslant \phi_{(h)}, h \in \mathbb{I}_p\right\}, \tag{6}$$

where $\mathbf{N} = \left[\mathbf{N}_{(1)}^T \; \mathbf{N}_{(2)}^T \cdots \mathbf{N}_{(p)}^T\right]^T \in \mathbb{R}^{p \times n_x}$ and $\boldsymbol{\phi} = \left[\phi_{(1)} \; \phi_{(2)} \cdots \phi_{(p)}\right]^T \in \mathbb{R}^p$ are known.

In region $\mathcal{O}$, consider that the system (2) can be exactly represented by a TS fuzzy model, described by the IF-THEN rules, where the φ-th fuzzy rule R^φ is given by

R^φ : IF $z_1(t)$ is M_1^φ AND $\cdots$ AND $z_{n_z}(t)$ is $M_{n_z}^\varphi$,
THEN $\dot{\mathbf{x}}(t) = \mathbf{A}_\varphi \mathbf{x}(t) + \mathbf{B}_\varphi u(t)$,

such that $\varphi \in \mathbb{I}_{n_r}$, M_j^φ is the j-th fuzzy set of the φ-th fuzzy rule, $j \in \mathbb{I}_{n_z}$ and $z_1(t), \cdots, z_{n_z}(t)$ are the premise variables.

More details about the exact representation of a nonlinear system by TS fuzzy models can be found in [43]. From this method, one obtains the following representation for the system (5):

$$\dot{\mathbf{x}}(t) = \mathbf{A}(\alpha)\mathbf{x}(t) + \mathbf{B}(\alpha)\ \text{sat}(\mathbf{u}(t)), \tag{7}$$

$$\mathbf{A}(\alpha) = \sum_{i=1}^{n_r} \alpha_i \mathbf{A}_i,\ \mathbf{B}(\alpha) = \sum_{i=1}^{n_r} \alpha_i \mathbf{B}_i,\ \sum_{i=1}^{n_r} \alpha_i = 1, \tag{8}$$

where $i \in \mathbb{I}_{n_r}$, $\mathbf{A}_i \in \mathbb{R}^{n_x \times n_x}$, $\mathbf{B}_i \in \mathbb{R}^{n_x \times n_u}$ and $\alpha_i = \alpha_i(\mathbf{z}(t))$.

Remark 1 The exact representation of an uncertain nonlinear system by a TS fuzzy model is guaranteed by the procedure presented in [44–47]. This procedure uses the lower and upper bounds of the system nonlinearities and uncertain linear terms considering the given operation region of the state vector and the known range of the plant uncertain parameters. Therefore, the TS fuzzy models obtained with this procedure can exactly represent uncertain nonlinear systems described in (5) by a TS fuzzy model (7), which presents known local models and uncertain normalized weights.

The next section shows the switched control design subject to saturation and presents LMIs conditions that are used to determine the feedback gains.

3 Robust Switched Control Design Subject to Actuator Saturation and Fault (RSwASF) for Fuzzy Systems

The robust switched control for the lower limb electrical stimulation is proposed considering the actuator saturation and fault under nonideal muscular conditions (fatigue, spasm and tremor).

The idea is to design a set of feedback gains, with only one gain used at each time, chosen based on a switching law that depends on the state vector of the controlled system. Fig. 1 shows the schema of the switched control for electrical stimulation.

Consider a nonlinear system subject to actuator saturation described by the following TS fuzzy model:

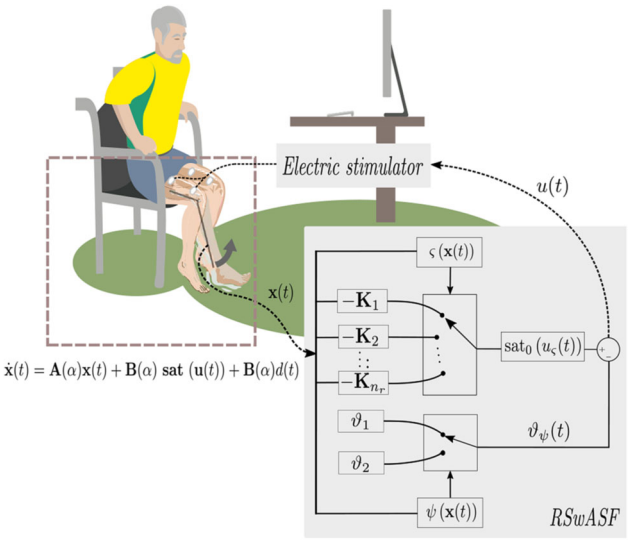

Fig. 1 Electrical stimulation system of the lower limbs using robust switched controller subject to actuator saturation and fault

$$\dot{\mathbf{x}} = \mathbf{A}(\alpha)\mathbf{x}(t) + \mathbf{B}(\alpha)\text{sat}(\mathbf{u}(t)) + \mathbf{B}(\alpha)d(t), \tag{9}$$

where $\mathbf{A}(\alpha)$ defined in (8), $\mathbf{B}(\alpha) = \mathbf{B}_0 g(\alpha)$, $g(\alpha) \geqslant 0$, for all α,

$$\begin{aligned} \text{sat}(\mathbf{u}(t)) &= \left[\text{sat}\left(u_{(1)}(t)\right) \cdots \text{sat}\left(u_{(n_u)}(t)\right)\right]^T, \\ \text{sat}\left(u_{(l)}(t)\right) &= \text{sgn}\left(\text{u}_{(\text{l})}(\text{t})\right)\min\left\{\rho_{(l)}, |\text{u}_{(\text{l})}(\text{t})|\right\}, \end{aligned} \tag{10}$$

$\forall l \in \mathbb{I}_{n_u}$, $\vartheta_1 \leqslant d(t) \leqslant \vartheta_2$, $\rho_{(l)}$ is the actuator saturation values.

We propose the application of the robust switched control law subject to actuator saturation. The proposed procedure uses a switching index ς, as described in (12, 13), which selects a state-feedback controller gain that belongs to the set $\left\{\mathbf{K}_j \in \mathbb{R}^{n_u \times n_x},\ j \in \mathbb{I}_{n_r}\right\}$ and an index ψ that compensates uncertainty in the signal control, as defined in (13). An index ς is determined by auxiliary symmetric matrices Q_j, obtained by the design procedure. The control law is defined as follows [44]:

$$\mathbf{u}(t) = \text{sat}_0(\mathbf{u}_\varsigma(t)) - \vartheta_\psi(t), \tag{11}$$

$$\mathbf{u}_\varsigma(t) = -\mathbf{K}_\varsigma \mathbf{x}(t), \tag{12}$$

$$\varsigma = \arg^* \min_{j \in \mathbb{I}_{n_r}} \left\{\mathbf{x}^T(t)\mathbf{Q}_j\mathbf{x}(t)\right\},\ \ \varsigma, \text{j} \in \mathbb{I}_{\text{n}_\text{r}}, \tag{13}$$

$$\psi = \arg^* \min_{m \in \mathbb{I}_2} \left\{-\mathbf{x}^T\mathbf{P}\mathbf{B}_0\vartheta_m\right\}, \tag{14}$$

where $\text{sat}_0(\mathbf{u}_\varsigma(t)) = \left[\text{sat}_0\left(u_{\varsigma(1)}(t)\right) \cdots \text{sat}_0\left(u_{\varsigma(n_u)}(t)\right)\right]^T$, and

$$\text{sat}_0\left(u_{\varsigma(l)}(t)\right) = \text{sgn}\left(\text{u}_{\varsigma(1)}(\text{t})\right)\min\left\{\rho_{0(1)}, |\text{u}_{\varsigma(1)}(\text{t})|\right\}, \tag{15}$$

where $\rho_{0(l)} = \rho_{(l)} - \max_{m \in \mathbb{I}_2}\{|\vartheta_m|\}$, $\forall l \in \mathbb{I}_{n_u}$, $m \in \mathbb{I}_2$, and ϑ_m, ρ, ρ_0, $\mathbf{B}_0$ will be defined later. The state-feedback matrices $\mathbf{K}_j$ and decision matrices $\mathbf{Q}_j$ will be obtained in the design procedure, ensuring the local stability of the system (9, 10, 11, 12, 13, 14 and 15) with decay rate.

In addition, consider the quadratic Lyapunov function $V(\mathbf{x}) = \mathbf{x}^T\mathbf{P}\mathbf{x}$, and let the ellipsoid $\mathcal{E}(\mathbf{P}, \delta)$

$$\mathcal{E}(\mathbf{P}, \delta) = \{\mathbf{x}(t) \in \mathbb{R}^{n_x} : \mathbf{x}(t)^T\mathbf{P}\mathbf{x}(t) \leqslant \delta\}, \tag{16}$$

where the constant $\delta > 0$.

An invariant region related to operating of the system is considered. The initial condition of the system, initiated in a suitable region within an operating region, will remain in this region for all $t \geqslant 0$. In other words, determining an invariant region, say $\mathcal{E} \subset \mathcal{O}$, $\forall \mathbf{x}(0) \in \mathcal{E}$, the state vector $\mathbf{x}(t)$ of (9) remains in the operating region $\mathcal{O}, \forall t \geqslant 0$. Consequently, (7) exactly represents system (5) for $t \geqslant 0$ and all $\mathbf{x}(0) \in \mathcal{E}$, following the procedure described in Sect. 2.1.

Lemma 1 [42, 44] *Consider a nonlinear system described by* (5) *and an operating region* $\mathbf{x}(t) \in \mathcal{O}$, *for* $t \geqslant 0$, *given in* (6). *Assume a symmetric positive definite matrix* $\mathbf{X} \in \mathbb{R}^{n_x \times n_x}$ *exists, such that*

$$\begin{bmatrix} \phi^2_{(h)} & \mathbf{N}_{(h)}\mathbf{X} \\ * & \mathbf{X} \end{bmatrix} \geqslant 0, \tag{17}$$

holds $\forall i$ and $h \in \mathbb{I}_p$, and $\mathbf{x}(t_1)^T\mathbf{P}\mathbf{x}(t_1)^T < \mathbf{x}(t_0)^T\mathbf{P}\mathbf{x}(t_0)^T$ for all $t_1 > t_0 > 0$, where $\mathbf{P} = \mathbf{X}^{-1}$. Therefore, if $\mathbf{x}(0) \in \mathcal{E}(\mathbf{P}, 1)$, given in (16), then $\mathbf{x}(t) \in \mathcal{O}$, $t \geqslant 0$.

Proof More details are found in [42, 44]. □

Consider the polyhedral set $\mathcal{L}(\mathbf{H}_k)$

$$\begin{aligned} \mathcal{L}(\mathbf{H}_k) := \Big\{\mathbf{x}(t) \in \mathbb{R}^{n_x} : \left|\mathbf{H}_{k(l)}\mathbf{x}(t)\right| \leqslant \breve{\rho}_{(l)},\ k \in \mathbb{I}_{n_r}, \\ \text{and } 1 \in \mathbb{I}_{\overrightarrow{\text{n}}_\text{u}}\Big\}, \end{aligned} \tag{18}$$

where $\breve{\boldsymbol{\rho}} = \left[\breve{\rho}_{(1)} \cdots \breve{\rho}_{(\overrightarrow{n}_u)}\right]^T \in \mathbb{R}^{\overrightarrow{n}_u}$, $\breve{\rho}_{(l)} > 0$, $\mathbf{H}_k = \left[\mathbf{H}^T_{k(1)} \cdots \mathbf{H}^T_{k(\overrightarrow{n}_u)}\right] \in R^{\overrightarrow{n}_u \times n_x}$ are known.

Consider the set $\mathcal{D}_{n_u}$ composed of 2^{n_u} diagonal matrices $\mathbf{D}_s \in \mathbb{R}^{n_u \times n_u}$, $s \in \mathbb{I}_{2^{n_u}}$, whose diagonal elements are either 1 or 0. For any $\mathbf{D}_s \in \mathcal{D}_{n_u}$, consider that $\mathbf{D}_s^- = \mathbf{I}_{n_u} - \mathbf{D}_s$.

Now, the function $q_{n_u} : \mathbb{I}_{2^{n_u}} \to \mathbb{I}_{2^{n_u}-1}$ is defined as follows:

$$\begin{cases} q_{n_u}(i_s) = q_{n_u}(i_s - 1) + 1, & \mathbf{D}_{i_s} + \mathbf{D}_{j_s} \neq \mathbf{I}_{n_u}, \\ & \forall j_s \in \mathbb{I}_{i_s},\ \text{i}_\text{s} \in \mathbb{I}_{2^{n_u}}, \\ q_{n_u}(i_s) = q_{n_u}(i_s), & \mathbf{D}_{i_s} + \mathbf{D}_{j_s} = \mathbf{I}_{n_u}, \\ & \exists j_s \in \mathbb{I}_{i_s},\ \text{i}_\text{s} \in \mathbb{I}_{2^{n_u}}. \end{cases} \tag{19}$$

This function will be useful for convex hull representation of saturation nonlinearity. In this paper, we adopted the saturation representation provided by [48].

Lemma 2 [48] *Let* $n_u \geqslant 1$ *be a given integer and* $\breve{\boldsymbol{\nu}} \in \mathbb{R}^{\overrightarrow{n}_u}$ *be such that* $\|\breve{\boldsymbol{\nu}}\|_\infty \leqslant \rho$, *where* $\|\breve{\boldsymbol{\nu}}\|_\infty = \max_{i \in \mathbb{I}_{\overrightarrow{n}_u}} |\breve{\nu}_i|$. *Let the*

elements in $\mathcal{D}_{n_u}$ *be labeled as* $\mathbf{D}_s$, $s \in \mathbb{I}_{2^{n_u}}$ *and the vector* $\mathbf{sl}_{2^{n_u-1},\, q_{n_u}(i_s)}$, *where the function* $q_{n_u}(i_s)$ *be defined in* (19). *Then, for any* $\mathbf{u} \in \mathbb{R}^{n_u}$, *there holds*

$$\text{sat}(\mathbf{u}) \in \text{co}\{\mathbf{D}_s\mathbf{u} + \mathbf{D}_s^- \boldsymbol{v}\},\ s \in \mathbb{I}_{2^{n_u}}, \tag{20}$$

if and only if, for any $\boldsymbol{\varrho} \in \mathbb{R}^{n_u}$

$$\begin{aligned}\langle \boldsymbol{\varrho}, \mathbf{sat}(\mathbf{u})\rangle \le \max_{s\in\mathbb{I}_{2^{n_u-1}}} \{&\langle \boldsymbol{\varrho}, \mathbf{D}_s\mathbf{u} + (\mathbf{sl}_{2^{n_u-1},\, s} \otimes \mathbf{D}_s^-)\breve{\boldsymbol{v}}\rangle,\\ &\langle \boldsymbol{\varrho}, \mathbf{D}_s^-\mathbf{u} + (\mathbf{sl}_{2^{n_u-1},\, s} \otimes \mathbf{D}_s)\breve{\boldsymbol{v}}\rangle\},\end{aligned} \tag{21}$$

where $\langle a_1, a_2\rangle$ denotes the inner product of the vectors a_1 and a_2, $\breve{\mathbf{D}}_s \in \mathbb{R}^{n_u \times \vec{\vec{n}}_u}$, which is defined as

$$\breve{\mathbf{D}}_s = \mathbf{sl}_{2^{n_u-1},\, q_{n_u}(i_s)} \otimes \mathbf{D}_s^-,\ \forall s, i_s \in \mathbb{I}_{2^{n_u}}. \tag{22}$$

Proof Further details are found in [48]. □

Remark 2 Note that Lemma 2 contains $\vec{\vec{n}}_u = n_u 2^{n_u-1}$ slack variables for the representation of the convex hull and usually offers less conservative conditions than that presented in [49].

For example, if $n_u = 2$, then $\vec{\vec{n}}_u = 4$, $\mathbf{D}_s$, $s \in \mathbb{I}_{2^{n_u}}$ are the matrices as follows:

$$\begin{aligned}&\text{sat}(\mathbf{u}) \in \text{co}\{\mathbf{D}_s\mathbf{u} + \mathbf{D}_s^- \boldsymbol{v}\},\ s \in \mathbb{I}_{2^{n_u}}.\\ &\mathcal{D}_2 = \{\mathbf{D}_1,\ \mathbf{D}_2,\ \mathbf{D}_3,\ \mathbf{D}_4\},\\ &\mathcal{D}_2 = \left\{\begin{bmatrix}1 & 0\\ 0 & 1\end{bmatrix}, \begin{bmatrix}1 & 0\\ 0 & 0\end{bmatrix}, \begin{bmatrix}0 & 0\\ 0 & 1\end{bmatrix}, \begin{bmatrix}0 & 0\\ 0 & 0\end{bmatrix}\right\}.\end{aligned} \tag{23}$$

From (19), adopting $q_2(0) = 0$, the associated function to elements of the set $\mathcal{D}_2$ is expressed as $q_2(1) = 1$, $q_2(2) = 2$, $q_2(3) = q_2(2) = 2$, and $q_2(4) = q_2(1) = 1$. Consequently, the row vectors are $\mathbf{sl}_{2,\, q_2(1)} = [1 \quad 0]$, $\mathbf{sl}_{2,\, q_2(2)} = [0 \quad 1]$, $\mathbf{sl}_{2,\, q_2(3)} = [0 \quad 1]$, and $\mathbf{sl}_{2,\, q_2(4)} = [1 \quad 0]$.

From (22) one obtains:

$$\begin{aligned}&\breve{\mathbf{D}}_s^- = \mathbf{sl}_{2,\, q_2(i_s)} \otimes \mathbf{D}_s^-,\ \forall s,\ i_s \in \mathbb{I}_4,\\ &\breve{\mathcal{D}}_2^- = \{\breve{\mathbf{D}}_1^-,\ \breve{\mathbf{D}}_2^-,\ \breve{\mathbf{D}}_3^-,\ \breve{\mathbf{D}}_4^-\},\\ &\breve{\mathcal{D}}_2^- = \left\{\begin{bmatrix}0 & 0 & 0 & 0\\ 0 & 0 & 0 & 0\end{bmatrix}, \begin{bmatrix}0 & 0 & 0 & 0\\ 0 & 0 & 0 & 1\end{bmatrix}, \begin{bmatrix}0 & 0 & 1 & 0\\ 0 & 0 & 0 & 0\end{bmatrix}, \begin{bmatrix}1 & 0 & 0 & 0\\ 0 & 1 & 0 & 0\end{bmatrix}\right\}.\end{aligned}$$

Thus, (20) can be written as

$$\mathbf{sat}(\mathbf{u}) \in \text{co}\left\{\begin{bmatrix}\text{u}_1\\ \text{u}_2\end{bmatrix}, \begin{bmatrix}\text{u}_1\\ \text{v}_4\end{bmatrix}, \begin{bmatrix}\text{v}_3\\ \text{u}_2\end{bmatrix}, \begin{bmatrix}\text{v}_1\\ \text{v}_2\end{bmatrix}\right\}.$$

Remark 3 If $\mathbf{x}(t) \in \mathcal{L}(\mathbf{H}_k)$ defined in (18), $k \in \mathbb{I}_{n_r}$, then $\mathbf{x}(t) \in \mathcal{L}(\mathbf{K}_j)$, $j \in \mathbb{I}_{n_r}$, and sat(u) can be rewritten as

$$\mathbf{sat}(\mathbf{u}) = \sum_{s=1}^{2^{n_u}} \lambda_s \left[\mathbf{D}_s\mathbf{u} + \breve{\mathbf{D}}_s^- \breve{\boldsymbol{v}}\right], \tag{24}$$

where $\mathbf{D}_s \in \mathcal{D}$, $\breve{\mathbf{D}}_s^- \in \breve{\mathcal{D}}^-$, $\breve{\mathbf{D}}_s^- = \mathbf{sl}_{2,\, q_2(i_s)} \otimes \mathbf{D}_s^-$, $s \in \mathbb{I}_{2^{n_u}}$, and $\lambda_s \geqslant 0$, $\sum_{s=1}^{2^{n_u}} \lambda_s = 1$.

Considering (15), $\rho_{0(l)} = \rho_{(l)} - \max_{m\in\mathbb{I}_2}\{|\vartheta_{m(l)}|\}$, from (11) one obtains $|u_{(l)}(t)| = |\text{sat}_0(u_{\varsigma(l)}(t)) - \vartheta_{\psi(l)}| \leqslant |\text{sat}_0(u_{\varsigma(l)}(t))| + |\vartheta_{\psi(l)}| \leqslant \rho_{0(l)} + \max\{\vartheta_{i(l)}\}$, $\rho_{0(l)} + \max\{\vartheta_{i(l)}\} = \rho_{(l)} + \max\{|\vartheta_i|\} - \max\{|\vartheta_i|\} = \rho_{(l)}$. Therefore

$$\begin{aligned}&\text{sat}(u_{(l)}(t)) = \text{sat}_0(u_{\varsigma(l)}(t)) - \vartheta_{\psi(l)}, \text{ and}\\ &\mathbf{sat}(\mathbf{u}(t)) = \mathbf{sat}_0(\mathbf{u}_\varsigma(t)) - \vartheta_\psi.\end{aligned}$$

Similarly to (24), if $\mathbf{x}(t) \in \mathcal{L}(\mathbf{H}_k)$, $k \in \mathbb{I}_{n_r}$, then $\mathbf{x}(t) \in \mathcal{L}(\mathbf{K}\varsigma)$ and $\mathbf{sat}_0(-\mathbf{K}_\varsigma\mathbf{x})$ one obtains

$$\mathbf{sat}_0(-\mathbf{K}_\varsigma\mathbf{x}) = \sum_{s=1}^{2^{n_u}} \lambda_s \left[\mathbf{D}_s(-\mathbf{K}_\varsigma\mathbf{x}) + \breve{\mathbf{D}}_s^-(\mathbf{H}_\varsigma\mathbf{x})\right]. \tag{25}$$

The following lemma provides a sufficient condition for the constraint $\mathcal{E}(\mathbf{P}, \delta) \subset \mathcal{L}(\mathbf{H}_k)$.

Lemma 3 [44, 49] *Let the sets* $\mathcal{E}(\mathbf{P}, \delta)$ *and* $\mathcal{L}(\mathbf{H}_k)$, *the constraint* $\mathcal{E}(\mathbf{P}, \delta) \subset \mathcal{L}(\mathbf{H}_k)$ *is enforced if the LMI*

$$\begin{bmatrix}\rho_{0(l)}^2\delta^{-1} & \mathbf{G}_{k(l)}\\ * & \mathbf{X}\end{bmatrix} \geqslant 0, \tag{26}$$

holds for all $k \in \mathbb{I}_{n_r}$, and $l \in \mathbb{I}_{\vec{\vec{n}}_u}$, where $\mathbf{X} = \mathbf{P}^{-1}$ and $\mathbf{G}_{k(l)} = \mathbf{H}_{k(l)}\mathbf{X}$.

Proof See [44, 49]. □

With all ellipsoids that satisfy the invariance condition, a less conservative choice of the largest ellipsoid inside the domain of attraction can be guaranteed considering its shape. Let $\mathcal{W}_0 \subset \mathbb{R}^{n_x}$ be defined as follows:

$$\mathcal{W}_0 = \text{co}\{\mathbf{w}_0^1,\ \mathbf{w}_0^2, \cdots, \mathbf{w}_0^q\}, \tag{27}$$

where $\mathbf{w}_0^{i_w} \in \mathbb{R}^{n_x}$, $\forall i_w \in \mathbb{I}_q$ are a priori given vectors.

A guarantee that a convex hull (27) is contained in the invariant region $\mathcal{E}(\mathbf{P}, 1)$ is described in Lemma 4.

Lemma 4 *The constraint* $\bar{\omega}\ \mathcal{W}_0 \subset \mathcal{E}(\mathbf{P}, 1)$, *where* $\mathcal{W}_0 = co\{\mathbf{w}_0^1, \mathbf{w}_0^2, \cdots, \mathbf{w}_0^q\}$, $\mathbf{w}_0^{i_w} \in \mathbb{R}^{n_x}$ *for all* $i_w \in I_q$, *is the convex hull of known vectors* $\mathbf{w}_0^1$, $\mathbf{w}_0^2$, $\cdots$, $\mathbf{w}_0^q$, *and the constant* $\bar{\omega} > 0$, *is enforced if*

$$\begin{bmatrix}\bar{\omega}^{-2} & \mathbf{w}_0^{kT}\\ \mathbf{w}_0^{i_w} & \mathbf{X}\end{bmatrix} \geqslant 0, \tag{28}$$

holds for all $i_w \in \mathbb{I}_q$. Thus, $\bar{\omega}$ can be used as a variable to obtain a less conservative estimate of the domain of attraction and to search the "largest" ellipsoid $\mathcal{E}(\mathbf{P}, 1)$.

Proof See [49, 50]. □

On the other hand, constraints may be adopted to avoid that the controller assumes a large norm, e.g., using Lemma 5.

Lemma 5 [44, 49] *It is possible to reduce the norm of the gain matrix* $\mathbf{K}_j$, $j \in \mathbb{I}_{n_r}$, *increasing the region* $\mathcal{L}(\mathbf{K}_j)$ *selecting appropriately* ξ *such that* $\mathcal{E}(\mathbf{P}, \xi^{-1}) \subset \mathcal{L}(\mathbf{K}_j)$ *is imposed if the LMI*

$$\begin{bmatrix} \xi \rho_{0(k)}^{-2} & \mathbf{M}_{j(k)} \\ * & \mathbf{X} \end{bmatrix} \geqslant 0, \tag{29}$$

holds for all $j \in \mathbb{I}_{n_r}$, and $k \in \mathbb{I}_{n_u}$.

Proof See [44, 49, 51]. □

Theorem 1 [44] *Let the sets* $\mathcal{E}(\mathbf{P}, 1)$, $\mathcal{L}(\mathbf{H}_k)$, *and* $\mathcal{W}_0$ *defined in* (16), (18), *and* (27), *respectively. Consider a nonlinear system subject to actuator saturation defined in* (9) *and* (10), *an operating region* $\mathbf{x}(t) \in \mathcal{O}$, *described by* (6), $t \geqslant 0$, $\boldsymbol{\rho} \in \mathbb{R}^{n_u}$, $\boldsymbol{\phi} \in \mathbb{R}^p$ *and* $\mathbf{N} \in \mathbb{R}^{p \times n_x}$ *are known. Assume that there exist a symmetric positive definite matrix* $\mathbf{X} \in \mathbb{R}^{n_x \times n_x}$, *symmetric matrices* $\bar{\mathbf{Q}}_i$ *and* $\bar{\mathbf{Z}}_i \in \mathbb{R}^{n_x \times n_x}$, *matrices* $\mathbf{G}_j = \left[G_{j(1)}^T \; G_{j(2)}^T \; \cdots G_{j(\bar{n}_u)}^T \right]$, $\mathbf{M}_i \in \mathbb{R}^{n_u \times n_x}$ *and a scalar* $\beta > 0$ *such that*

$$\mathbf{A}_i \mathbf{X} + \mathbf{X} \mathbf{A}_i^T + \bar{\mathbf{Z}}_i + \bar{\mathbf{Q}}_i + 2\beta \mathbf{X} < 0, \tag{30}$$

$$\begin{aligned} &- \mathbf{B}_i \mathbf{D}_s \mathbf{M}_j + \mathbf{B}_i \breve{\mathbf{D}}_s^{-} \mathbf{G}_j - \mathbf{M}_j^T \mathbf{D}_s^T \mathbf{B}_i^T \\ &\quad + \mathbf{G}_j^T \breve{\mathbf{D}}_s^{-T} \mathbf{B}_i^T - \bar{\mathbf{Z}}_i - \bar{\mathbf{Q}}_j \leqslant 0, \end{aligned} \tag{31}$$

$$\begin{bmatrix} \rho_{0(l)}^2 & \mathbf{G}_{j(l)} \\ * & \mathbf{X} \end{bmatrix} \geqslant 0, \tag{32}$$

$$\begin{bmatrix} \phi_{(h)}^2 & \mathbf{N}_{(h)} \mathbf{X} \\ * & \mathbf{X} \end{bmatrix} \geqslant 0, \tag{33}$$

$$\begin{bmatrix} \xi \rho_{0(k)}^{-2} & \mathbf{M}_{i(k)} \\ * & \mathbf{X} \end{bmatrix} \geqslant 0, \tag{34}$$

$$\begin{bmatrix} \bar{w}^{-2} & * \\ \mathbf{w}_0^{i_w} & \mathbf{X} \end{bmatrix} \geqslant 0, \tag{35}$$

hold for all i and $j \in \mathbb{I}_{n_r}$, $k \in \mathbb{I}_{n_u}$, $l \in \mathbb{I}_{\bar{n}_u}$ $h \in \mathbb{I}_p$, $i_w \in \mathbb{I}_q$, $s \in \mathbb{I}_{2^{n_u}}$, $\mathbf{D}_s \in \mathcal{D}$ and $\breve{\mathbf{D}}_s^{-} \in \breve{\mathcal{D}}$. Then, the control law (11, 12, 13, 14 and 15), where $\mathbf{K}_i = \mathbf{M}_i \mathbf{X}^{-1}$ and $\mathbf{Q}_i = \mathbf{X}^{-1} \bar{\mathbf{Q}}_i \mathbf{X}^{-1}$ for all $i \in \mathbb{I}_{n_r}$, makes the system (9) locally asymptotically stable with a decay rate equal to or greater than β, $\forall \mathbf{x}(0) \in \mathcal{E}(\mathbf{P}, 1)$, where $\mathbf{P} = \mathbf{X}^{-1}$. Furthermore, $\mathbf{x}(t) \in \mathcal{O}$, $t \geqslant 0$.

Proof Based on [44], consider as Lyapunov function candidate $V(\mathbf{x}(t)) = \mathbf{x}(t)^T \mathbf{P} \mathbf{x}(t)$, $\mathbf{P} = \mathbf{P}^T \in \mathbb{R}^{n_x \times n_x}$, $\mathbf{P} > 0$. Therefore, from the system (9) and the control law (12)

$$\begin{aligned} \dot{V}(\mathbf{x}) &= 2\mathbf{x}^T \mathbf{P} \dot{\mathbf{x}}, \\ &= 2\mathbf{x}^T \mathbf{P} [\mathbf{A}(\alpha)\mathbf{x} + \mathbf{B}(\alpha) \mathrm{sat}(\mathbf{u}) + \mathbf{B}(\alpha) d]. \end{aligned} \tag{36}$$

Replacing (11, 12) in (36)

$$\begin{aligned} \dot{V}(\mathbf{x}) &= 2\mathbf{x}^T \mathbf{P} \mathbf{A}(\alpha)\mathbf{x} + 2\mathbf{x}^T \mathbf{P} \mathbf{B}(\alpha) \left[\mathrm{sat}_0(\mathbf{u}_\varsigma(t)) - \vartheta_\psi(t) \right] \\ &\quad + 2\mathbf{x}^T \mathbf{P} \mathbf{B}(\alpha) d, \\ \dot{V}(\mathbf{x}) &= 2\mathbf{x}^T \mathbf{P} \mathbf{A}(\alpha)\mathbf{x} + 2\mathbf{x}^T \mathbf{P} \mathbf{B}(\alpha) \mathbf{sat}_0(-\mathbf{K}_\varsigma \mathbf{x}) \\ &\quad + 2\mathbf{x}^T \mathbf{P} \mathbf{B}(\alpha) \left[d - \vartheta_\psi(t) \right]. \end{aligned} \tag{37}$$

Considering (25), (37) can be rewritten as

$$\begin{aligned} \dot{V}(\mathbf{x}) &= 2\mathbf{x}^T \mathbf{P} \mathbf{A}(\alpha)\mathbf{x} + 2\mathbf{x}^T \mathbf{P} \mathbf{B}(\alpha) \left[d - \vartheta_\psi \right] \\ &\quad + 2\mathbf{x}^T \mathbf{P} \mathbf{B}(\alpha) \left\{ \sum_{s=1}^{2^{n_u}} \lambda_s \left[\mathbf{D}_s(-\mathbf{K}_\varsigma \mathbf{x}) + \breve{\mathbf{D}}_s^{-}(\mathbf{H}_\varsigma \mathbf{x}) \right] \right\}. \end{aligned}$$

Note that $\vartheta_1 \leqslant d(t) \leqslant \vartheta_2$ can be described as a convex combination $\sum_{m=1}^{2} \gamma_m(t) = 1$, $\gamma_1(t), \gamma_2(t) \geqslant 0$, $\gamma_2(t) = \frac{d(t) - \vartheta_1}{\vartheta_2 - \vartheta_1}$, $\gamma_1(t) = 1 - \gamma_2(t)$.

Therefore, replacing $\mathbf{B}(\alpha) = \mathbf{B}_0 g(\mathbf{x})$, $g(\mathbf{x}) \geqslant 0$, $\forall \mathbf{x} \neq 0$, from (14), it follows that

$$\begin{aligned} &\mathbf{x}^T \mathbf{P} \mathbf{B}(\alpha) \left[d - \vartheta_\psi \right] \\ &\quad = \mathbf{x}^T \mathbf{P} \mathbf{B}_0 \left[\sum_{m=1}^{2} \gamma_m(t) \vartheta_m + \min_{m \in \mathbb{I}_2} \left\{ -\mathbf{x}^T \mathbf{P} \mathbf{B}_0 \vartheta_m \right\} \right] \\ &\quad \leqslant \mathbf{x}^T \mathbf{P} \mathbf{B}_0 \sum_{m=1}^{2} \gamma_m(t) \vartheta_m - \mathbf{x}^T \mathbf{P} \mathbf{B}_0 \sum_{m=1}^{2} \gamma_m(t) \vartheta_m = 0. \end{aligned} \tag{38}$$

Then, from (38) one obtains

$$\begin{aligned} \dot{V}(\mathbf{x}) &\leqslant \mathbf{x}^T \left[\mathbf{A}(\alpha)^T \mathbf{P} + \mathbf{P} \mathbf{A}(\alpha) \right] \mathbf{x} \\ &\quad + \left\{ \sum_{s=1}^{2^{n_u}} \lambda_s \left[\mathbf{D}_s(-\mathbf{K}_\varsigma \mathbf{x}) + \breve{\mathbf{D}}_s^{-}(\mathbf{H}_\varsigma \mathbf{x}) \right] \right\}^T \mathbf{B}(\alpha)^T \mathbf{P} \mathbf{x} \\ &\quad + \mathbf{x}^T \mathbf{P} \mathbf{B}(\alpha) \left\{ \sum_{s=1}^{2^{n_u}} \lambda_s \left[\mathbf{D}_s(-\mathbf{K}_\varsigma \mathbf{x}) + \breve{\mathbf{D}}_s^{-}(\mathbf{H}_\varsigma \mathbf{x}) \right] \right\}. \end{aligned} \tag{39}$$

Now, assume that there exist symmetric matrices $\mathbf{Z}_i$ and $\mathbf{Q}_j$ such that

$$\begin{aligned} &\left[-\mathbf{D}_s \mathbf{K}_j + \breve{\mathbf{D}}_s^{-} \mathbf{H}_j \right]^T \mathbf{B}_i^T \mathbf{P} \\ &\quad + \mathbf{P} \mathbf{B}_i \left[-\mathbf{D}_s \mathbf{K}_j + \breve{\mathbf{D}}_s^{-} \mathbf{H}_j \right] \leqslant \mathbf{Z}_i + \mathbf{Q}_j, \end{aligned} \tag{40}$$

$\forall i, j \in \mathbb{I}_{n_r}$, $\forall \mathbf{D}_s \in \mathcal{D}$, and $\forall \breve{\mathbf{D}}_s^{-} \in \breve{\mathcal{D}}^{-}$. Then, for $j = \varsigma$, multiplying by α_i, where $\alpha_i \geqslant 0$, and taking the sum from $i = 1$ to n_r, $\sum_{i=1}^{n_r} \alpha_i = 1$ and then multiplying the result by λ_s, $\lambda_s \geqslant 0$ and taking the sum from $s = 1$ to 2^{n_u}, $\sum_{s=1}^{2^{n_u}} \lambda_s = 1$, considering $\mathbf{B}(\alpha) = \sum_{i=1}^{n_r} \alpha_i \mathbf{B}_i$, $\alpha_i \geqslant 0$, $\sum_{i=1}^{n_r} \alpha_i = 1$, $i \in \mathbb{I}_{n_r}$ one has

$$\sum_{s=1}^{2^{n_u}} \lambda_s \Big\{ \left[-\mathbf{D}_s\mathbf{K}_\varsigma + \breve{\mathbf{D}}_s^{-}\mathbf{H}_\varsigma\right]^T \mathbf{B}(\alpha)^T\mathbf{P} + \mathbf{P}\mathbf{B}(\alpha)\left[-\mathbf{D}_s\mathbf{K}_\varsigma + \breve{\mathbf{D}}_s^{-}\mathbf{H}_\varsigma\right] \Big\} \leqslant \mathbf{Z}(\alpha) + \mathbf{Q}_\varsigma, \tag{41}$$

where $\mathbf{Z}(\alpha) = \sum_{i=1}^{n_r} \alpha_i \mathbf{Z}_i$. Note that, from the control law (13), $\mathbf{x}^T\mathbf{Q}_\varsigma\mathbf{x} = \min_{i\in\mathbb{I}_{n_r}}\{\mathbf{x}^T\mathbf{Q}_i\mathbf{x}\} \leqslant \sum_{i=1}^{n_r} \alpha_i\mathbf{x}^T\mathbf{Q}_i\mathbf{x} = \mathbf{x}^T\mathbf{Q}(\alpha)\mathbf{x}$.

Thus, from (39) and (41),

$$\dot{V}(\mathbf{x}) \leqslant \mathbf{x}^T\left\{\mathbf{A}(\alpha)^T\mathbf{P} + \mathbf{P}\mathbf{A}(\alpha) + \mathbf{Z}(\alpha) + \mathbf{Q}(\alpha)\right\}\mathbf{x}. \tag{42}$$

Aiming to achieve a decay rate greater than or equal to β it is sufficient that $\dot{V}(\mathbf{x}) \leqslant -2\beta V(\mathbf{x})$ [51]. Hence, from (42) is sufficient that, $\forall i \in \mathbb{I}_{n_r}$,

$$\mathbf{A}_i^T\mathbf{P} + \mathbf{P}\mathbf{A}_i + \mathbf{Z}_i + \mathbf{Q}_i + 2\beta\mathbf{P} \leqslant 0. \tag{43}$$

Premultiplying and postmultiplying (40) and (43) by $\mathbf{X} = \mathbf{P}^{-1}$ and performing the change of variables $\mathbf{G}_j = \mathbf{H}_j\mathbf{X}$, $\mathbf{M}_j = \mathbf{K}_j\mathbf{X}$, $\bar{\mathbf{Z}}_i = \mathbf{X}\mathbf{Z}_i\mathbf{X}$ and $\bar{\mathbf{Q}}_i = \mathbf{X}\mathbf{Q}_i\mathbf{X}$, one obtains (30) and (31). Note that as $V(\mathbf{x}) = \mathbf{x}^T\mathbf{P}\mathbf{x}$ and $\dot{V}(\mathbf{x}) < 0$, $\mathbf{x} \neq 0$, from (16), if $\mathbf{x}(0) \in \mathcal{E}(\mathbf{P}, \delta)$ then $\mathbf{x}(t) \in \mathcal{E}(\mathbf{P}, \delta)$, $\forall t \geqslant 0$. Considering Lemma 3 with $\delta = 1$, LMI (32) ensure $\mathcal{E}(\mathbf{P}, 1) \subset \mathcal{L}(\mathbf{H}_k)$, a sufficient condition such that (25) holds. And considering Lemma 1, LMI (33) ensure $\mathcal{E}(\mathbf{P}, 1) \subset \mathcal{O}$, a sufficient condition for a state trajectory started with an initial condition $\mathbf{x}(0) \in \mathcal{E}(\mathbf{P}, 1)$ remains in $\mathcal{O}$ for all $t \geqslant 0$. In addition, considering Lemma 4, LMI (35) guarantees that the convex hull (27) is contained in the invariant region $\mathcal{E}(\mathbf{P}, 1)$, and LMI (34) minimizes the norm of the matrices $\mathbf{K}_i$, selecting appropriately ξ such that $\mathcal{E}(\mathbf{P}, \xi^{-1}) \subset \mathcal{L}(\mathbf{K}_i)$. The proof is complete. □

Remark 4 The Gaino et al. approach [4] treated the plant model without uncertainties. Consequently, the values of $\breve{u}^d$ and nominal torque M_a are not uncertain. Now, assuming nonidealities, the state vector becomes an estimate, since M_a^d is uncertain. However, a term $\vartheta_\psi(t)$ that will dominate the error from the uncertainty of the desired torque, was added to the control signal. Thus,

$$\breve{u} = -\mathbf{K}_\varsigma\mathbf{x}_e(t) + \vartheta_\psi(t), \tag{44}$$

where $\mathbf{x}_e(t) = [x_1(t)\ x_2(t)\ x_{3e}(t)]^T$, $x_{3e}(t) = \breve{x}_3 - M_{a\,nom}^d$, $M_{a\,nom}$ is the nominal torque and $\mathbf{K}_\varsigma = [K_{\varsigma 1}\ K_{\varsigma 2}\ K_{\varsigma 3}]$.

Considering the following relationship $x_{3e}(t) = \breve{x}_3 - M_a^d + \Delta M_a$, $\Delta M_a = M_a^d - M_{a\,nom}^d$, (44) can be rewritten as

$$\breve{u} = -[K_{\varsigma 1} \quad K_{\varsigma 2} \quad K_{\varsigma 3}]\begin{bmatrix} x_1 \\ x_2 \\ x_3 + \Delta M_a \end{bmatrix} + \vartheta_\psi(t),$$

Therefore,

$$u = \breve{u} - \breve{u}_e^d,$$

$$u = -[K_{\varsigma 1} \quad K_{\varsigma 2} \quad K_{\varsigma 3}]\begin{bmatrix} x_1 \\ x_2 \\ x_3 \end{bmatrix} - K_{\varsigma 3}\Delta M_a - \breve{u}_e^d + \vartheta_\psi(t),$$

$$u = -\mathbf{K}_\varsigma\mathbf{x} - \breve{u}^d + u_{error} + \vartheta_\psi(t),$$

where $u_{error} = \left(\breve{u}^d - \breve{u}_e^d - K_{\varsigma 3}\Delta M_a\right)$ will be dominated by the term $\vartheta_\psi(t)$ from the control law (11), where $\vartheta_1 \leqslant \vartheta_\psi(t) \leqslant \vartheta_2$, $\vartheta_1 = \min\{\breve{u}^d\}$ and $\vartheta_2 = \max\{\breve{u}^d\}$, $\breve{u}^d$ defined in (3).

3.1 Example: Paraplegic Individual P3

Table 1 presents the parameter values for healthy and paraplegic individuals, corresponding to experimental tests conducted by Ferrarin et al. [40].

Consider the operating region defined in the interval $0 \leqslant \breve{x}_1(t) \leqslant \frac{7\pi}{18}$, desired position belongs to set $\theta^d \in [\pi/6 \quad \pi/3]$, $\max\{M_a^d\} = 9.16$, and the uncertain parameters $\hat{G} \in [0.9G_n \quad G_n]$, $\kappa_{stf} \in [0.1 \quad 1]$, and $\kappa_{flt} \in [0.8 \quad 1]$.

Observe that the system (4) has three uncertain nonlinear functions $\tilde{f}_{21}(\mathbf{z}(t))$, $\tilde{f}_{23}(\mathbf{z}(t))$, and $\tilde{g}_{31}(\mathbf{z}(t))$, consequently one obtains $n_r = 2^3 = 8$.

Table 1 Parameters from healthy and paraplegic individuals [40]

Parameter	H1	H2	H3	H4	H5	P1	P2	P3
J [kg m^2]	0.377	0.358	0.399	0.375	0.384	0.362	0.292	0.394
m [kg]	4.05	4.63	4.38	3.83	4.36	4.37	3.42	4.76
l [m]	0.253	0.239	0.248	0.237	0.243	0.238	0.231	0.233
B [N m s/rad]	0.377	0.311	0.400	0.305	0.332	0.270	0.302	0.289
λ [N m/rad]	1.199	4.679	3.657	4.490	3.889	41.208	3.761	15.352
E_v [rad^{-1}]	− 0.486	0.041	− 0.031	0.257	− 0.079	2.024	1.317	1.644
ω [rad]	2.548	2.427	2.710	2.701	2.412	2.918	2.520	3.896
G_n [N m/A]	266.67	266.67	256.67	266.67	333.33	283.33	83.33	76.67
τ [s]	0.454	0.426	0.491	0.406	0.438	0.951	0.203	0.215

To find the local models, the maximum and minimum values of the uncertain nonlinear functions must be obtained.

Considering the paraplegic individual P3, whose parameters can be found in Table 1, and taking $\mathbf{x} = \check{\mathbf{x}} - \check{\mathbf{x}}_e$, the set $\mathbb{D}$ is obtained

$$\mathbb{D} = \Big\{ z \in \mathbb{R}^6 : -\frac{\pi}{3} \leqslant x_1 \leqslant \frac{4\pi}{18},\ -M_a^d \leqslant x_3 \leqslant M_a^d,\ 0.9G_n \leqslant \hat{G} \leqslant G_n,\ 0.1 \leqslant \kappa_{stf} \leqslant 1,\ 0.8 \leqslant \kappa_{flt} \leqslant 1, \frac{\pi}{6} \leqslant \theta^d \leqslant \frac{\pi}{3} \Big\}.$$

Consequently, one obtains the local models for exact representation of system (4) through TS fuzzy models (7), $\rho = 150$, and

$$\mathbf{A}_1 = \mathbf{A}_2 = \begin{bmatrix} 0 & 1 & 0 \\ 25.7877 & -0.7335 & 2.5381 \\ 0 & 0 & -4.6512 \end{bmatrix},$$

$$\mathbf{A}_3 = \mathbf{A}_4 = \begin{bmatrix} 0 & 1 & 0 \\ 25.7877 & -0.7335 & 0.2538 \\ 0 & 0 & -4.6512 \end{bmatrix},$$

$$\mathbf{A}_5 = \mathbf{A}_6 = \begin{bmatrix} 0 & 1 & 0 \\ 1.6826 & -0.7335 & 2.5381 \\ 0 & 0 & -4.6512 \end{bmatrix},$$

$$\mathbf{A}_7 = \mathbf{A}_8 = \begin{bmatrix} 0 & 1 & 0 \\ 1.6826 & -0.7335 & 0.2538 \\ 0 & 0 & -4.6512 \end{bmatrix},$$

$$\mathbf{B}_1 = \mathbf{B}_3 = \mathbf{B}_5 = \mathbf{B}_7 = \begin{bmatrix} 0 \\ 0 \\ 1.4264 \times 10^3 \end{bmatrix},$$

$$\mathbf{B}_2 = \mathbf{B}_4 = \mathbf{B}_6 = \mathbf{B}_8 = \begin{bmatrix} 0 \\ 0 \\ 1.0270 \times 10^3 \end{bmatrix}.$$

The operating region $\mathcal{O}$ is described by (6), where $p = 3$, $\mathbf{N} = \mathbf{I}_3$, and $\boldsymbol{\phi} = [\frac{\pi}{3} \quad 4 \quad 10]^T$. Moreover, note that $\mathbf{B}(\alpha) = \mathbf{B}_0 g(\mathbf{z})$, where $\mathbf{B}_0 = [0 \quad 0 \quad 1]^T$, and $g(\mathbf{z}) \geqslant 0$, $g_0(\mathbf{z}) = \max_{\mathbf{z} \in \mathbb{D}} \{g(\mathbf{z})\} = 1.4264 \times 10^3$.

The LMIs (30) were solved using the MATLAB software, and the modeling language YALMIP [52] with the solver LMILab [53]. Solving the LMIs (27) presented in Theorem 1, the aforementioned parameters, $\beta = 4.0$, $q = 4$, $\mathbf{w}_0^1 = [\frac{\pi}{6} \quad 0 \quad 9.16]^T$, $\mathbf{w}_0^2 = [\frac{\pi}{6} \quad 0 \quad -9.16]^T$, $\mathbf{w}_0^3 = [-\frac{\pi}{18} \quad 0 \quad 9.16]^T$, $\mathbf{w}_0^4 = [-\frac{\pi}{18} \quad 0 \quad -9.16]^T$, $\vartheta_1 = \min\{\breve{u}^d\} = 0.0149$, $\vartheta_2 = \max\{\breve{u}^d\} = 0.0332$, $\rho_0 = 0.150$ minimizing $\bar{w}$, one obtains the gains of the proposed RSwASF control procedure:

Table 2 RMS error between control techniques for healthy ($RMSE_h$) and paraplegic ($RMSE_p$) individuals considering nonidealities (severe). *BC* backstepping control, *DPID* double-proportional-integral-derivative, *GSC* gain-scheduling control, *IBC* integral-backstepping control, *PDC* parallel distributed compensation, *PID* proportional-integral-derivative control, *SMC* sliding-mode control, *ST* super-twisting, *RSwASF* robust switched control subject to actuator saturation and fault. N_h and N_p denote the numbers of the healthy and paraplegic individuals. Bold font indicates best result obtained

Controller	N_h	N_p	$RMSE_h$ [deg]	$RMSE_p$ [deg]
PID	1	3	12.27	14.88
GSC	1	3	11.73	12.46
SMC	1	3	7.44	13.16
DPID	1	3	8.68	9.64
BC	1	3	6.79	8.73
IBC	1	3	8.30	9.05
ST	1	3	6.69	7.25
PDC	5	3	16.09	22.37
RPDC	5	3	8.37	16.94
RSwASF	5	3	**3.75**	**5.16**

$$\mathbf{P} = \begin{bmatrix} 7.8226 \times 10^4 & 1.1754 \times 10^4 & 196.7513 \\ 1.1754 \times 10^4 & 2.0495 \times 10^4 & 33.6308 \\ 196.7513 & 33.6308 & 0.8309 \end{bmatrix},$$

$$\mathbf{K}_1 = [0.5406 \quad 0.0956 \quad 0.0027],$$
$$\mathbf{K}_2 = [0.5365 \quad 0.0967 \quad 0.0028],$$
$$\mathbf{K}_3 = [0.6319 \quad 0.1082 \quad 0.0026],$$
$$\mathbf{K}_4 = [0.6511 \quad 0.1128 \quad 0.0027],$$
$$\mathbf{K}_5 = [0.5220 \quad 0.0954 \quad 0.0027],$$
$$\mathbf{K}_6 = [0.5129 \quad 0.0963 \quad 0.0027],$$
$$\mathbf{K}_7 = [0.6165 \quad 0.1091 \quad 0.0026],$$
$$\mathbf{K}_8 = [0.6238 \quad 0.1120 \quad 0.0027].$$

The TS fuzzy control techniques PDC and RPDC were comparated using the LMIs presented by Gaino et al. [4] and Covacic et al. [35], respectively. Solving the LMIS presented by Covacic et al. [35], considering the values $\mu = 150$ mA, $\beta = 4.0$, and the constraint of the operating region (17), one obtains the following:

(a) Muscle nonidealities in mild conditions.

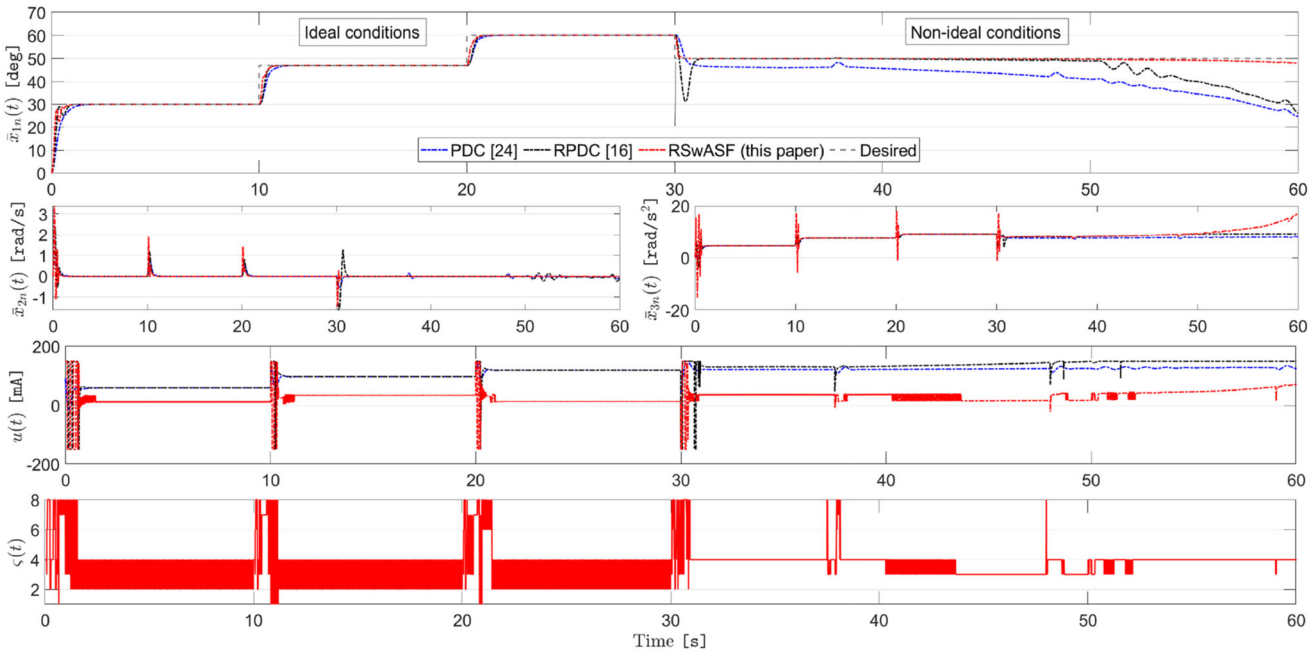

(b) Muscle nonidealities in severe conditions and actuator fault.

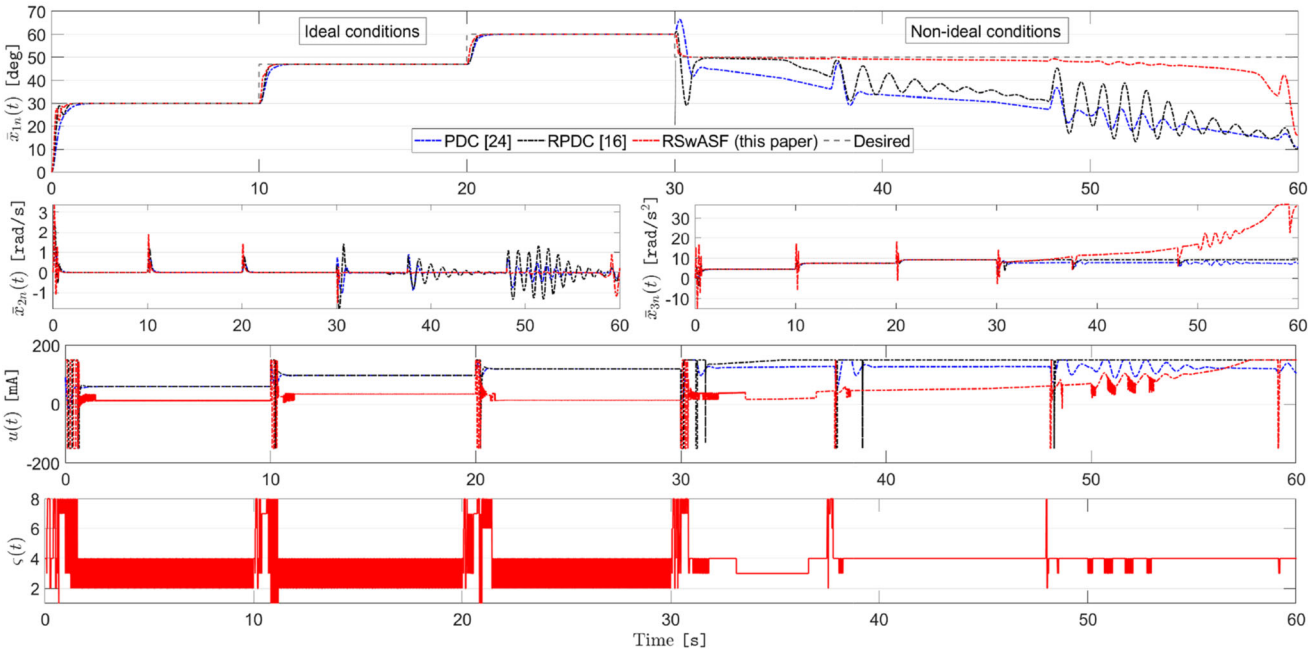

Fig. 2 Lower limb dynamic behavior for muscle nonidealities (fatigue, spasms, and tremor) in **a** mild and **b** severe conditions and considering actuator fault (80% of the nominal)

$$\mathbf{Q} = \begin{bmatrix} 1.9071 \times 10^{12} & 2.7137 \times 10^{11} & 3.5540 \times 10^{7} \\ 2.7137 \times 10^{11} & 5.0976 \times 10^{10} & 6.7066 \times 10^{6} \\ 3.5540 \times 10^{7} & 6.7066 \times 10^{6} & 5.3648 \times 10^{5} \end{bmatrix},$$

$$\mathbf{P} = \begin{bmatrix} 40.6894 & 7.1150 & 1.4004 \\ 7.1150 & 1.3163 & 0.2534 \\ 1.4004 & 0.2534 & 0.0621 \end{bmatrix},$$

$$\mathbf{K}_1 = \mathbf{M}_1\mathbf{X} = \begin{bmatrix} 48.7925 & 9.1864 & 0.7267 \end{bmatrix},$$
$$\mathbf{K}_2 = \mathbf{M}_2\mathbf{X} = \begin{bmatrix} 47.4738 & 8.9370 & 0.7230 \end{bmatrix},$$
$$\mathbf{F}_1 = \mathbf{M}_1\mathbf{X} = \begin{bmatrix} 0.0058 & 0.0011 & 2.3611 \times 10^{-4} \end{bmatrix},$$
$$\mathbf{F}_2 = \mathbf{M}_2\mathbf{X} = \begin{bmatrix} 0.0047 & 0.0010 & 2.1859 \times 10^{-4} \end{bmatrix}.$$

$\epsilon_{11} = 1.9786 \times 10^{-10}$, $\epsilon_{12} = 1.9415 \times 10^{-10}$, $\epsilon_{22} = 1.8969 \times 10^{-10}$.

The LMIs presented by Gaino et al. [4] were solved considering the values $\mu = 150$ mA, $\beta = 4.0$, and constraint for operating region (17). Consequently, one obtains the following:

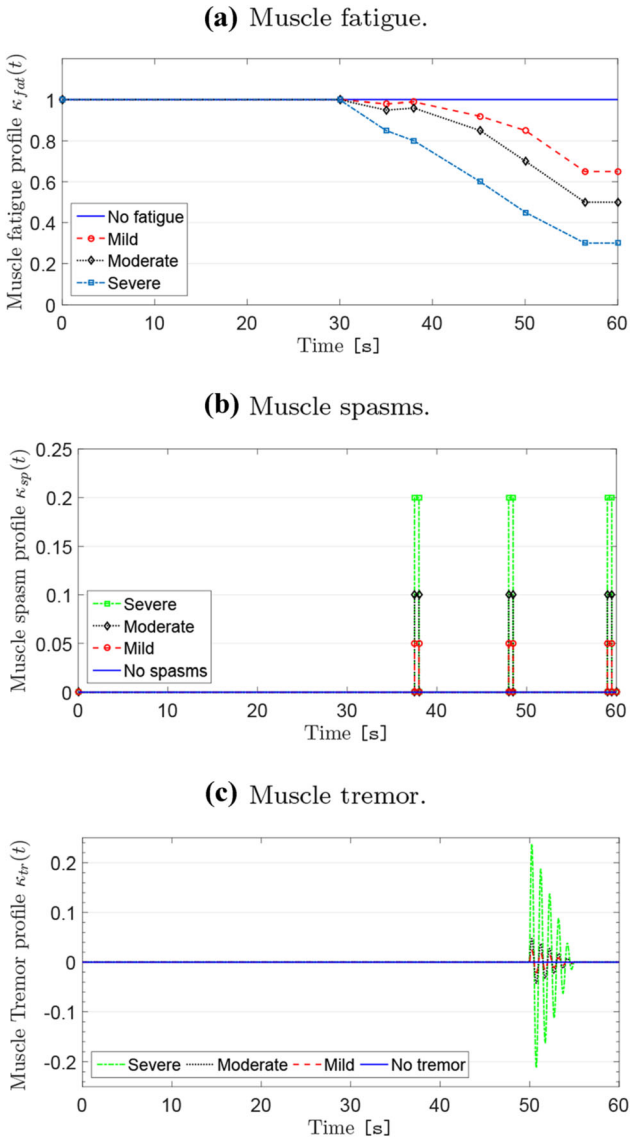

Fig. 3 Muscle behavior in different nonidealities levels inserted during the tests: **a** fatigue, **b** spasms, and **c** tremor

4 Results and Discussion

Usually, the results of controllers from simulation consider ideal conditions for electrical stimulation of the lower limbs, i.e., without fatigue, tremor, spasms, and other uncertainties. First, we present the results under ideal conditions. Next, we evaluated the nonideal conditions. A priori, the comparative study was carried out using TS fuzzy-based control techniques. The results obtained from other techniques in the literature were then compared.

4.1 Ideal Conditions

Three operating points in the time interval $0 \leqslant t \leqslant 30$ s were evaluated considering the plant in ideal conditions. Fig. 2 shows the regulation performance of PDC [4], RPDC [35], and RSwASF (proposed) control techniques, using the gains designed in Sect. 3.1.

The root-mean-squared error value in the steady state (*SSRMSE*) was rated. For the three studied controllers, considering all individuals, the steady-state performance was satisfactory for regulation to the desired operating point. The null steady-state error was obtained.

4.2 Nonideal Conditions

The actuator fault, parametric uncertainty in the muscular recruitment function, and the different levels of fatigue, spasms, and tremor were simulated.

4.2.1 Muscle Fatigue, Tremor and Spasms

Muscle nonidealities (fatigue, spasms, and tremor) alter muscle torque. These nonidealities were evaluated in the time interval $30 < t \leqslant 60$ s (Fig. 3). Note that the muscle fatigue profile is a decreasing function in the temporal domain, indicating a reduced muscular torque. Spasms profiles are described as torque impulses, which change the dynamics of the system for a short time. The tremor indicates damped torque oscillations, and its amplitude is strictly related to the degree of severity.

Figure 2a and b illustrate the system performance considering mild and severe condition of muscular nonidealities, respectively.

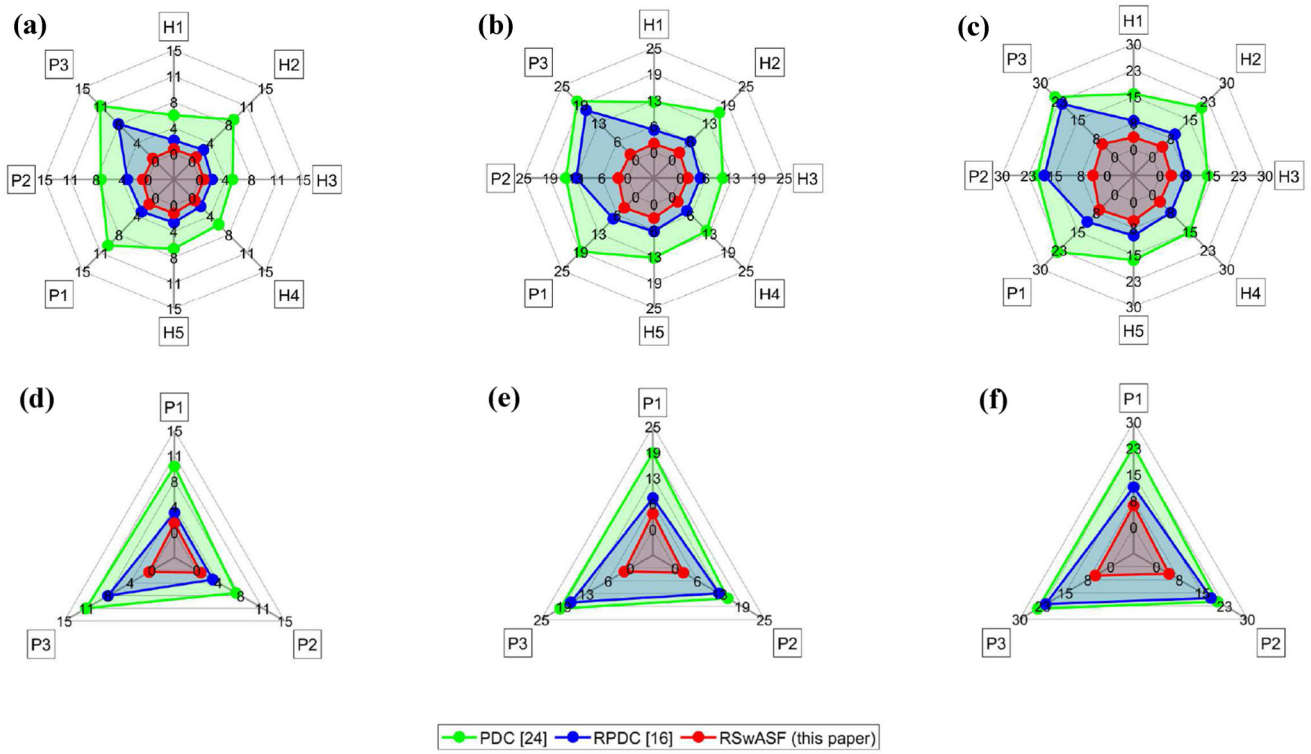

Fig. 4 Comparison of RMS error between PDC [4], RPDC [35], and RSwASF (this paper) control techniques, considering healthy (*Hi*) and paraplegic (*Pj*) individuals in different scenarios of nonidealities: **a** fatigue—mild; **b** fatigue—moderate; **c** fatigue—severe; **d** fatigue, spasms, and tremor—mild; **e** fatigue, spasms and tremor—moderate; **and f** fatigue, spasms, and tremor—severe

The nonideality situations due to fatigue are listed first. Fatigue, spasms, and tremor were assessed at three levels: mild, moderate and severe.

Note that although the RSwASF controller reduces the steady-state error, the fatigue precludes the null error. The muscle torque is substantially reduced. Consequently, maintaining the angular position and muscular activation applied to a single motor point is a difficult task, because the fatigue effect modifies the musculoskeletal system to null torque. One way to get better results is to stimulate more than one muscle activation point, switching the channels by detecting fatigue [2] or other events.

For all individuals, the highest RMS error was obtained for the severe fatigue situation (Fig. 4). This condition presents a greater error than considering all nonidealities in maximum severity degree. This behavior is due to spasticity [41]. In this case, spasticity effectively increases the knee joint stiffness, contributing to a smaller error in the controllers' performance.

4.2.2 Actuator Fault and Parametric Uncertainty in the Muscle Recruitment

The actuator fault was considered as a decrease in energy (80% of the nominal) applied to the muscles. An uncertainty in the muscular recruitment function, expressed by parameter $\hat{G}$, was also assumed.

The RSwASF controller reached the desired operating point, even in the presence of parametric uncertainties (Fig. 2b).

Regarding the results obtained among the TS fuzzy techniques, the RSwASF controller presented the best performance.

4.3 Comparative Analysis with Literature

The comparison between control techniques considering the nonidealities in the plant model is considered for isometric application of electrical stimulation. The knee joint controlled in a single angular position is a therapy to obtain muscle strength through electrical stimuli [31]. In this sense, the goal of the closed-loop system to obtain regulation with the smallest RMS error in different angular positions.

Table 2 lists the *RMSE* between different control techniques in the literature. Control techniques whose plant model considered parametric uncertainties in severe conditions were evaluated. Lynch and Popovic [41] initiated this modeling approach. First, the PID and sliding-mode (SMC) controllers were compared. In severe conditions of fatigue, spasms, and tremor, the RMS errors were large for

both controllers. Next, Lynch and Popovic [39] proposed a comparative analysis with the gain-scheduling controller (GSC). Among the controllers, the PDC [4] had the worst performance. The PDC [4] obtained a large RMS error and was more sensitive to parametric variation. The SMC produced a relatively large RMS error. Although it is a robust technique, it was sensitive to parametric variation. This result may be due to the use of the boundary layer control, which compromised the convergence properties. In turn, the GSC produced a better response and less sensitivity to uncertainties, because it used integral control. An unfavorable point of the GSC refers to lengthy tuning process the multiple local controllers.

Benahmed et al. [1] proposed an analysis with other controllers. The double-PID (DPID) reduced *RMSE*, when compared to the PID, but errors persisted due to sensitivity to plant parameters. Regarding sensitivity, backstepping (BC), integral-backstepping (IBC), and super-twisting (ST) were also evaluated. The sensitivity of BC to variations in parameters was lower than IBC and ST. On the other hand, adding integral action, there is a reduction in the *RMSE* index, but the sensitivity deteriorates.

Before this study, the technique that established the least *RMSE* was the ST [1]. The RSwASF controller surpassed the ST and obtained the best result, achieving the lowest *RMSE* for the angular position, considering all individuals and in all nonideal conditions.

About TS fuzzy technique, the PDC and RPDC controllers, proposed by Gaino et al. [4] and Covacic et al. [35], respectively, present unsatisfactory behavior (Fig. 2), since they do not deal with plant uncertainties. Although Covacic et al. [35] proposed a norm-bounded uncertainty control, it is worth mentioning that the authors did not consider that the moment of inertia parameter is an uncertainty in the nonlinear function $f_{21}(z)$. Consequently the TS model of the system is inaccurate.

In relation to actuator fault and parametric uncertainty, the results indicate a discrepancy between the knee angular position and the desired value using the PDC [4] and RPDC [35]. The incompatibility between the model and control design explains the degraded performance.

4.4 Advantages and Limitations of the RSwASF

The RSwASF handled uncertainties inherent in the individual, such as muscle fatigue, spasms, tremor, and also features of the system such as saturation and actuator failure. Under ideal conditions, the performance of the PDC [4], RPDC [35], and RSwASF are similar. However, under nonideal conditions, the RSwASF controller performed better in the tests compared with the PDC [4].

Considering a nonlinear system described by the TS fuzzy model, the PDC controller depends on the known membership functions. The expressions of the membership functions can be extensive and demand a high computational cost to calculate them. When dealing with uncertain systems, the result obtained with PDC becomes unsatisfactory, because the membership functions become unsuitable for model uncertainties. Thus, the RSwASF controller is presented as an advantageous proposal, since it does not depend explicitly on the membership functions for the convex combination of controller gains. Other switched control applications for uncertain nonlinear plants can be found in [44, 45, 47].

It is worth mentioning that there is chattering in the control signal from the RSwASF under ideal conditions. However, this behavior can be smoothed using a smooth function, proposed by Alves et al. [44]. Nonetheless, this function was not needed in relation to nonideal conditions.

5 Conclusions

The uncertainty of the recruitment function, actuator fault, and other nonideality parameters add an error to the model, specifically to nominal torque $M^d_{a\,nom}$ and in the value of u^d. This analysis explains why different muscle torque estimation-based control techniques yield regulation error.

The novelty of this study was the RSwASF control law applied to compensate plant uncertainties. This technique was compared to other control techniques in the literature. Among control techniques, the PDC presented the highest *RMSE*, followed by the PID and GSC. The RMS error has been reduced through a robust approach based on TS fuzzy models; however, its performance was below the sliding-mode control, ST, and backstepping control. The best performance among all reported techniques was presented by RSwASF, which using TS fuzzy models properly dealt with uncertainties and nonidealities of the system.

The contribution of this study was the improvement of the performance of the isometric contraction evoked by electrical stimuli dealing under nonideal conditions (fatigue, spasms, tremor, muscular activation and actuator saturation, and fault), as uncertainties in the control design.

Future works may investigate a new mathematical model for the plant, relating muscle activation and kinematic variables appropriately without relying on muscle torque estimation. From this study, hybrid FES systems such as powered ankle–foot prostheses [54] can be investigated, as well as isotonic applications with insertion of the delay effect in the plant through an approach proposed by [55].

Acknowledgements This study was financed in part by the CAPES (Coordenação de Aperfeiçoamento de Pessoal de Nível Superior - Brasil) - Finance Code 001; by the Brazilian National Council for

Scientific and Technological Development (CNPq) under research fellowships 309.872/2018-9 and 312.170/2018-1. The authors would like to thank Enago for English language review.

Declaration

Conflict of interest The authors declare no conflict of interest.

References

1. Benahmed, S., Tadjine, M., Kermia, O.: Comparative study of non-linear controllers for the regulation of the paraplegic knee movement using functional electrical stimulation. J. Mech. Med. Biol. **18**(05), 1850019 (2018). https://doi.org/10.1142/S0219519418500197
2. Downey, R.J., Cheng, T.H., Bellman, M.J., Dixon, W.E.: Switched tracking control of the lower limb during asynchronous neuromuscular electrical stimulation: theory and experiments. IEEE Trans. Cybern. **47**(5), 1251–1262 (2017). https://doi.org/10.1109/TCYB.2016.2543699
3. Gaino, R., Covacic, M.R., Cardim, R., Sanches, M.A.A., De Carvalho, A.A., Biazeto, A.R., Teixeira, M.C.M.: Discrete Takagi-Sugeno fuzzy models applied to control the knee joint movement of paraplegic patients. IEEE Access **8**, 32714–32726 (2020). https://doi.org/10.1109/ACCESS.2020.2971908
4. Gaino, R., Covacic, M.R., Teixeira, M.C.M., Cardim, R., Assunção, E., de Carvalho, A.A., Sanches, M.A.A.: Electrical stimulation tracking control for paraplegic patients using T-S fuzzy models. Fuzzy Sets Syst. **314**, 1–23 (2017). https://doi.org/10.1016/j.fss.2016.06.005
5. Kirsch, N., Alibeji, N., Sharma, N.: Nonlinear model predictive control of functional electrical stimulation. Control Eng. Pract. **58**, 319–331 (2017). https://doi.org/10.1016/j.conengprac.2016.03.005
6. Teodoro, R.G., Nunes, W.R.B.M., de Araujo, R.A., Sanches, M.A.A., Teixeira, M.C.M., Carvalho, A.A.D.: Robust switched control design for electrically stimulated lower limbs: a linear model analysis in healthy and spinal cord injured subjects. Control Eng. Pract. **102**, 104530 (2020). https://doi.org/10.1016/j.conengprac.2020.104530
7. Yang, R., de Queiroz, M.: Robust adaptive control of the nonlinearly parameterized human shank dynamics for electrical stimulation applications. J. Dyn. Syst. Meas. Control **140**(8), 1–15 (2018). https://doi.org/10.1115/1.4039366
8. Bao, X., Molazadeh, V., Dodson, A., Dicianno, B.E., Sharma, N.: Using person-specific muscle fatigue characteristics to optimally allocate control in a hybrid exoskeleton-preliminary results. IEEE Trans. Med. Robot. Bion. **2**(2), 226–235 (2020). https://doi.org/10.1109/TMRB.2020.2977416
9. Bao, X., Molazadeh, V., Dodson, A.: Model predictive control-based knee actuator allocation during a standing-up motion with a powered. Adv. Motor Neuroprosthese (2020). https://doi.org/10.1007/978-3-030-38740-2_6
10. Kobravi, H.R., Erfanian, A.: A decentralized adaptive fuzzy robust strategy for control of upright standing posture in paraplegia using functional electrical stimulation. Med. Eng. Phys. **34**(1), 28–37 (2012). https://doi.org/10.1016/j.medengphy.2011.06.013
11. Riener, R., Fuhr, T.: Patient-driven control of FES-supported standing up: a simulation study. IEEE Trans. Rehabil. Eng. **6**(2), 113–124 (1998). https://doi.org/10.1109/86.681177
12. Bo, A.P.L., Lopes, A.C.G., da Fonseca, L.O., Ochoa-Diaz, C., Azevedo-Coste, C., Fachin-Martins, E.: Experimental results and design considerations for FES-assisted transfer for people with spinal cord injury. Springer, Cham (2019). https://doi.org/10.1007/978-3-030-01845-0_189
13. Jovic, J., Azevedo Coste, C., Fraisse, P., Henkous, S., Fattal, C.: Coordinating upper and lower body during FES-assisted transfers in persons with spinal cord injury in order to reduce arm support. Neuromodul. Technol. Neural Interface **18**(8), 736–743 (2015). https://doi.org/10.1111/ner.12286
14. Jovic, J., Bonnet, V., Fattal, C., Fraisse, P., Coste, C.A.: A new 3d center of mass control approach for FES-assisted standing: first experimental evaluation with a humanoid robot. Med. Eng. Phys. **38**(11), 1270–1278 (2016). https://doi.org/10.1016/j.medengphy.2016.09.002
15. de Abreu, D.C.C., Cliquet, A., Rondina, J.M., Cendes, F.: Electrical stimulation during gait promotes increase of muscle cross-sectional area in quadriplegics: a preliminary study. Clin. Orthop. Related Res. **467**(2), 553 (2009). https://doi.org/10.1007/s11999-008-0496-9
16. Alibeji, N., Kirsch, N., Sharma, N.: An adaptive low-dimensional control to compensate for actuator redundancy and fes-induced muscle fatigue in a hybrid neuroprosthesis. Control Eng. Pract. **59**, 204–219 (2017). https://doi.org/10.1016/j.conengprac.2016.07.015
17. Alibeji, N.A., Molazadeh, V., Dicianno, B.E., Sharma, N.: A control scheme that uses dynamic postural synergies to coordinate a hybrid walking neuroprosthesis: theory and experiments. Front. Neurosci. **12**, 159 (2018). https://doi.org/10.3389/fnins.2018.00159
18. Granat, M., Ferguson, A., Andrews, B., Delargy, M.: The role of functional electrical stimulation in the rehabilitation of patients with incomplete spinal cord injury-observed benefits during gait studies. Spinal Cord **31**(4), 207–215 (1993). https://doi.org/10.1038/sc.1993.39
19. Ha, K.H., Murray, S.A., Goldfarb, M.: An approach for the cooperative control of FES with a powered exoskeleton during level walking for persons with paraplegia. IEEE Trans. Neural Syst. Rehabil. Eng. **24**(4), 455–466 (2016). https://doi.org/10.1109/TNSRE.2015.2421052
20. Kirsch, N.A., Bao, X., Alibeji, N.A., Dicianno, B.E., Sharma, N.: Model-based dynamic control allocation in a hybrid neuroprosthesis. IEEE Trans. Neural Syst. Rehabil. Eng. **26**(1), 224–232 (2017). https://doi.org/10.1109/TNSRE.2017.2756023
21. Kralj, A., Bajd, T., Turk, R.: Enhancement of gait restoration in spinal injured patients by functional electrical stimulation. Clin. Orthop. Relat. Res. **233**, 34–43 (1988)
22. Sharma, N., Mushahwar, V., Stein, R.: Dynamic optimization of FES and orthosis-based walking using simple models. IEEE Trans. Neural Syst. Rehabil. Eng. **22**(1), 114–126 (2014). https://doi.org/10.1109/TNSRE.2013.2280520
23. Wiesener, C., Axelgaard, J., Horton, R., Niedeggen, A., Schauer, T.: Functional electrical stimulation assisted swimming for paraplegics. In: 22nd Annual IFESS Conference, pp. 1–4 (2018)
24. Wiesener, C., Spieker, L., Axelgaard, J., Horton, R., Niedeggen, A., Wenger, N., Seel, T., Schauer, T.: Supporting front crawl swimming in paraplegics using electrical stimulation: a feasibility study. Journal of NeuroEngineering and Rehabilitation **17**, 1–14 (2020). https://doi.org/10.1186/s12984-020-00682-6
25. Andrews, B., Gibbons, R., Wheeler, G.: Development of functional electrical stimulation rowing: the rowstim series. Artif. Organs **41**(11), E203–E212 (2017). https://doi.org/10.1111/aor.13053
26. Lambach, R.L., Stafford, N.E., Kolesar, J.A., Kiratli, B.J., Creasey, G.H., Gibbons, R.S., Andrews, B.J., Beaupre, G.S.: Bone changes in the lower limbs from participation in an fes rowing exercise program implemented within two years after traumatic spinal cord injury. J. Spinal Cord Med. **43**(3), 306–314 (2020). https://doi.org/10.1080/10790268.2018.1544879

27. Bellman, M.J., Cheng, T.H., Downey, R.J., Hass, C.J., Dixon, W.E.: Switched control of cadence during stationary cycling induced by functional electrical stimulation. IEEE Trans. Neural Syst. Rehabil. Eng. **24**(12), 1373–1383 (2016). https://doi.org/10.1109/TNSRE.2015.2500180
28. Bo, A.P.L., da Fonseca, L.O., Guimaraes, J.A., Fachin-Martins, E., Paredes, M.E.G., Brindeiro, G.A., de Sousa, A.C.C., Dorado, M.C.N., Ramos, F.M.: Cycling with spinal cord injury: a novel system for cycling using electrical stimulation for individuals with paraplegia, and preparation for Cybathlon 2016. IEEE Robot. Autom. Mag. **24**(4), 58–65 (2017). https://doi.org/10.1109/MRA.2017.2751660
29. Fonseca, L.O., Bó, A.P., Guimarães, J.A., Gutierrez, M.E., Fachin-Martins, E.: Cadence tracking and disturbance rejection in functional electrical stimulation cycling for paraplegic subjects: a case study. Artif. Organs **41**(11), E185–E195 (2017). https://doi.org/10.1111/aor.13055
30. McDaniel, J., Lombardo, L.M., Foglyano, K.M., Marasco, P.D., Triolo, R.J.: Setting the pace: insights and advancements gained while preparing for an FES bike race. J. NeuroEng. Rehabil. **14**(1), 1–8 (2017). https://doi.org/10.1186/s12984-017-0326-y
31. Marquez-Chin, C., Popovic, M.R.: Functional electrical stimulation therapy for restoration of motor function after spinal cord injury and stroke: a review. BioMed. Eng. Online **19**, 1–25 (2020). https://doi.org/10.1186/s12938-020-00773-4
32. Ferrarin, M., Palazzo, F., Riener, R., Quintern, J.: Model-based control of FES induced single joint movements. IEEE Trans. Neural Syst. Rehabil. Eng. **9**(3), 245–257 (2001). https://doi.org/10.1109/7333.948452
33. Ferrante, S., Pedrocchi, A., Iannò, M., De Momi, E., Ferrarin, M., Ferrigno, G.: Functional electrical stimulation controlled by artificial neural networks: pilot experiments with simple movements are promising for rehabilitation applications. Functi. Neurol. **19**(4), 243–252 (2004)
34. Sharma, N., Kirsch, N.A., Alibeji, N.A., Dixon, W.E.: A nonlinear control method to compensate for muscle fatigue during neuromuscular electrical stimulation. Front. Robot. AI **4**, 68 (2017). https://doi.org/10.3389/frobt.2017.00068
35. Covacic, M.R., Teixeira, M.C.M., Carvalho, A.A.D., Cardim, R., Assunção, E., Sanches, M.A.A., Fujimoto, H.S., Mineo, M.S., Biazeto, A.R., Gaino, R.: Robust TS fuzzy control of electrostimulation for paraplegic patients considering norm-bounded uncertainties. Math. Probl. Eng. (2020). https://doi.org/10.1155/2020/4624657
36. Mohammed, S., Poignet, P., Fraisse, P., Guiraud, D.: Toward lower limbs movement restoration with input-output feedback linearization and model predictive control through functional electrical stimulation. Control Eng. Pract. **20**(2), 182–195 (2012). https://doi.org/10.1016/J.CONENGPRAC.2011.10.010
37. Wang, Q., Sharma, N., Johnson, M., Gregory, C.M., Dixon, W.E.: Adaptive inverse optimal neuromuscular electrical stimulation. IEEE Trans. Cybern. **43**(6), 1710–1718 (2013). https://doi.org/10.1109/TSMCB.2012.2228259
38. Ajoudani, A., Erfanian, A.: A neuro-sliding mode control with adaptive modeling of uncertainty for control of movement in paralyzed limbs using functional electrical stimulation. IEEE Trans. Biomed. Eng. **56**(7), 1771–1780 (2009). https://doi.org/10.1109/TBME.2009.2017030
39. Lynch, C.L., Popovic, M.R.: A comparison of closed-loop control algorithms for regulating electrically stimulated knee movements in individuals with spinal cord injury. IEEE Trans. Neural Syst. Rehabil. Eng. **20**(4), 539–548 (2012). https://doi.org/10.1109/TNSRE.2012.2185065
40. Ferrarin, M., Pedotti, A.: The relationship between electrical stimulus and joint torque: a dynamic model. IEEE Tran. Rehabil. Eng. **8**(3), 342–352 (2000). https://doi.org/10.1109/86.867876
41. Lynch, C.L., Graham, G.M., Popovic, M.R.: A generic model of real-world non-ideal behaviour of FES-induced muscle contractions: simulation tool. J. Neural Eng. (2011). https://doi.org/10.1088/1741-2560/8/4/046034
42. Klug, M., Castelan, E.B., Leite, V.J., Silva, L.F.: Fuzzy dynamic output feedback control through nonlinear Takagi-Sugeno models. Fuzzy Sets Syst. **263**, 92–111 (2015). https://doi.org/10.1016/J.FSS.2014.05.019
43. Taniguchi, T., Tanaka, K., Ohtake, H., Wang, H.O.: Model construction, rule reduction, and robust compensation for generalized form of Takagi-Sugeno fuzzy systems. IEEE Trans. Fuzzy Syst. **9**(4), 525–538 (2001). https://doi.org/10.1109/91.940966
44. Alves, U.N.L.T., Teixeira, M.C.M., Oliveira, D.R., Cardim, R., Assunção, E., Souza, W.A.D.: Smoothing switched control laws for uncertain nonlinear systems subject to actuator saturation. Int. J. Adapt. Control Signal Process. **30**(8–10), 1408–1433 (2016). https://doi.org/10.1002/acs.2671
45. de Oliveira, D.R., Teixeira, M.C.M., Alves, U.N.L.T., de Souza, W.A., Assunção, E., Cardim, R.: On local Hoo switched controller design for uncertain T-S fuzzy systems subject to actuator saturation with unknown membership functions. Fuzzy Sets Syst. **1**, 1–26 (2017). https://doi.org/10.1016/j.fss.2017.12.004
46. Santim, M.P.A., Teixeira, M.C.M., Souza, W.A.D., Cardim, R., Assuncao, E.: Design of a Takagi-Sugeno fuzzy regulator for a set of operation points. Math. Probl. Eng. (2012). https://doi.org/10.1155/2012/731298
47. Souza, W.A.D., Teixeira, M.C.M., Cardim, R., Assunção, E.: On switched regulator design of uncertain nonlinear systems using Takagi-Sugeno fuzzy models. IEEE Trans. Fuzzy Syst. **22**(6), 1720–1727 (2014). https://doi.org/10.1109/TFUZZ.2014.2302494
48. Zhou, B.: Analysis and design of discrete-time linear systems with nested actuator saturations. Syst. Control Lett. **62**(10), 871–879 (2013). https://doi.org/10.1016/J.SYSCONLE.2013.06.012
49. Hu, T., Lin, Z., Chen, B.M.: An analysis and design method for linear systems subject to actuator saturation and disturbance. Automatica **38**, 351–359 (2002). https://doi.org/10.1016/S0005-1098(01)00209-6
50. Cao, Y.Y., Lin, Z.: Robust stability analysis and fuzzy-scheduling control for nonlinear systems subject to actuator saturation. IEEE Trans. Fuzzy Syst. **11**(1), 57–67 (2003). https://doi.org/10.1109/TFUZZ.2002.806317
51. Boyd, S., Ghaoui, L.E., Feron, E., Balakrishnan, V.: Linear matrix inequalities in system and control theory, 15th edn. SIAM, Portland (1994)
52. Lofberg, J.: YALMIP: A toolbox for modeling and optimization in MATLAB. In: 2004 IEEE International Symposium on Robotics and Automation, pp. 284–289. IEEE (2004). https://doi.org/10.1109/CACSD.2004.1393890
53. Gahinet, P., Nemirovskii, A., Laub, A.J., Chilali, M.: The LMI control toolbox. In: Proceedings of the 1994 33rd IEEE Conference on Decision and Control, vol. 3, pp. 2038–2041. IEEE (1994). https://doi.org/10.1109/CDC.1994.411440
54. Al Kouzbary, M., Abu Osman, N.A., Al Kouzbary, H., Shasmin, H.N., Arifin, N.: Towards universal control system for powered ankle-foot prosthesis: a simulation study. Int. J. Fuzzy Syst. **22**(4), 1299–1313 (2020). https://doi.org/10.1007/s40815-020-00855-4
55. Wang, G., Jia, R., Song, H., Liu, J.: Stabilization of unknown nonlinear systems with TS fuzzy model and dynamic delay partition. J. Intell. Fuzzy Syst. **35**(2), 2079–2090 (2018). https://doi.org/10.3233/JIFS-172012

Willian Ricardo Bispo Murbak Nunes was born in Londrina, Brazil. He received the B.S. and M. Sc. degree in Electrical Engineering from the Londrina State University Londrina (UEL), Brazil, in 2012 and 2015, respectively. He received the Specialist degree in Industrial Automation Engineering from the SENAI in 2014, and the D.Sc. degree in electrical engineering from the São Paulo State University (UNESP), Ilha Solteira (FEIS), Brazil, in 2019, with a focus on the development of robust control systems for applications involving functional electrical stimulation, specifically those involving rehabilitation and mobility of the lower extremities. He was awarded at the Knowledge Olympics 2009, Industrial Electronic. Currently he is professor in the Federal University of Technology - Paraná (UTFPR). His research interests lie in fuzzy systems, robust and switched systems, and electronic instrumentation for Electrical and Biomedical Engineering applications.

Uiliam Nelson Lendzion Tomaz Alves graduated in Control and Automation Engineering from UniCesumar, Maringá, PR, Brazil (2011). He did his MSc. and PhD. in Electrical Engineering from UNESP (Universidade Estadual Paulista), Campus of Ilha Solteira, SP, Brazil, in 2014 and 2017, respectively. At this moment, he is a Control and Industrial Processes professor in IFPR (Instituto Federal de Educação, Ciência e Tecnologia do Paraná), campus Jacarezinho. His research interests include Fuzzy modeling and control, robust and nonlinear control.

Marcelo Augusto Assunção Sanches was born in São José do Rio Preto, Brazil. In 2002, he received the B.Sc from UNIFEB, in 2007 M.Sc., and 2013 the D.Sc. from the University of the State of São Paulo (UNESP), all in electrical engineering. In 2011, he held Sandwich Doctorate at the Fondazione Don Carlo Gnocchi Technology Center, Milan, Italy (CNPq - SWE Fellow). He has experience in research in the electrical engineering, acting on the following subjects electronic instrumentation, biomedical instrumentation, rehabilitation engineering, control and instrumentation, microcontrollers, extensometer, and electrostimulation. He is currently a Professor with the Department of Electrical Engineering and Postgraduate Program in electrical engineering at Univ Estadual Paulista (UNESP).

Marcelo Carvalho Minhoto Teixeira was born in Campo Grande, Brazil, in 1957. He received the B.Sc. degree in electrical engineering from the Escola de Engenharia de Lins, Lins, Brazil, in 1979, the M.Sc. degree in electrical engineering from the Instituto Alberto Luiz Coimbra de Pós-graduação e Pesquisa de Engenharia, Universidade Federal do Rio de Janeiro, Rio de Janeiro, Brazil, in 1982, and the D.Sc. degree in electrical engineering from Pontifícia Universidade Católica do Rio de Janeiro, Rio de Janeiro, in 1989. In 1982, he joined the Department of Electrical Engineering, Univ Estadual Paulista (UNESP), Ilha Solteira (FEIS), Brazil, where he is currently a Professor. In 1996 and 1997, he was a Visiting Scholar at the School of Electrical and Computer Engineering, Purdue University, West Lafayette, IN, USA. He was a Coordinator, from 2005 to 2007 and a Vice Coordinator, from 2000 to 2005 and from 2007 to 2010 of the Postgraduate Program in electrical engineering at FEIS-UNESP. He was a member of the Brazilian Evaluation Committee of Postgraduate Courses IV Engineering CAPES, from 2009 to 2013. Additionally, he was the Coordinator, from 1991 to 1993, and a Vice Coordinator, from 1989 to 1991 and from 1993 to 1995 of the Undergraduate Program in electrical engineering at FEIS-UNESP. He was an Associate Editor for the IEEE TRANSACTIONS ON FUZZY SYSTEMS, from 2016 to 2020. His interests include control theory and applications, neural networks, variable-structure systems, linear-matrix-inequality-based designs, fuzzy systems, nonlinear systems, adaptive systems, and switched systems.

Aparecido Augusto de Carvalho received the B.S degree in electrical engineering from the University of S ao Paulo (1976), the M.S degree in biomedical engineering from Federal University of Rio de Janeiro (1979) and the Ph.D degree in Physics from the University of S ao Paulo (1987). From 1993 to 1994, he was a Postdoctoral Scientist with the University of Wisconsin-Madison, investigating a method for measuring of x-ray intensity in the medical diagnostic range by pyroelectric sensors and a method for extending the practical range of conductive polymer sensors for measuring contact force. He started his career as an Assistant Professor with the Department of Electrical Engineering, Sao Paulo State University - UNESP, Brazil, in 1980. Since 2005, he has been a Full Professor. He was member of the Advisory Committee of the National Council for Scientific and Technological Development - CNPq (Brazil) in the area of Electrical and Biomedical Engineering, from 2008 to 2010. He was Secretary of the Brazilian Society of Biomedical Engineering in the 2011-2012 biennium. He was a member of the Superior Council of the Biomedical Engineering Center of Campinas State University from 2010 to 2014. His research interests include biomedical instrumentation, rehabilitation engineering, and functional electrical stimulation (FES).